ORIGINAL RESEARCH ARTICLE

DC Ferrochrome Smelting: The Arcing Zone and Its Influence on Energy Transport and Exergy Dissipation

HARMEN OTERDOOM, MARKUS REUTER, and JOHAN ZIETSMAN

Phenomena between the electrode tip, the arc attachment zone (AAZ), and the bath below the AAZ—taken together as arc attachment volume (AAV)—have a significant impact on the performance and efficiency of DC arc furnaces. This paper investigates the phenomena in the AAV in detail. Phenomena are analyzed with reference to industrial scale furnace *viz*. a Kazakh DC ferrochrome furnace. The impact of the various reactions in the AAV under different conditions both from an energy and exergy flow perspective is analyzed. The temperature, carbon in feed (thus the carbon to feed ratio called RC), and slag from the slag bath are investigated as the significant variables affecting phenomena in the AAV. Results show that alloy can become the reductant to fume specifically Mg(g), SiO(g), Cr(g) and even Fe(g) from slag containing MgO SiO_2, FeO_x and Cr_2O_3. The implications and resulting mass and energy transfer by these fumes can play a significant role in understanding open-bath ferrochrome smelting better as well as the energy balance of the arc and its impact on overall furnace efficiency. The irreversibility of the fuming reactions and reoxidation of metal vapor has a significant negative impact on furnace operation if the temperature in the AAV is not managed well due to poor operation regarding charging of feed. This implies not only that the average slag and metal temperature are of importance, but especially the actual AAV temperature is crucial. To fully understand the effect of chemical potential of the gases coming from the AAV, an exergy analysis uniquely showed that the fumes can be essential to reduce energy consumption if managed well, especially if the chemical potential energy can be harnessed in other zones within the furnace. This investigation is also relevant to other open-bath processes with fumable oxides, for example in smelting of ferronickel, titania slag, direct reduced iron, or even iron ore. Understanding the reaction mechanisms in the AAV in detail will be significant to push efficiencies of these applications to their thermodynamic, kinetic, and technological limits to ensure that their green metallurgical impact is fully realized.

https://doi.org/10.1007/s11663-024-03365-y

I. INTRODUCTION

FERROCHROME (FeCr) is produced from chrome-containing ore that has the generalized mineralogy $(Fe,Mg)O{\cdot}(Al,Cr,Fe)_2O_3$. Gangue material typically consists of magnesium silicates.[1,2] Chromite ore can occur as massive lumps, friable lumps, and fine material.

The most common path of FeCr production is in an alternating current (AC) submerged-arc furnace (SAF) applying a burden operation. Such a burden requires a permeable feed mix for which lump ore or agglomerated material is needed. Fine ore can be processed into pellets or briquettes.

HARMEN OTERDOOM is with the Department of Materials Science and Metallurgical Engineering, University of Pretoria, Lynnwood Road, Pretoria 0081, South Africa and also with the Butter Bridge, Boumanstraat 6, Groningen 9724 BR, Netherlands. Contact e-mail: harmen.oterdoom@butterbridge.eu MARKUS REUTER is with the Faculty of Science and Engineering, Curtin University, Kent Street, Perth 6102, Australia. JOHAN ZIETSMAN is with the Department of Materials Science and Metallurgical Engineering, University of Pretoria and also with the Ex Mente, 448, Monica Road, Pretoria 0081, South Africa.

Markus Reuter and Johan Zietsman have contributed meaningfully and substantially to this work.

Manuscript submitted July 11, 2024; accepted October 27, 2024.

Article published online December 12, 2024.

In direct current (DC) furnaces the feed material falls directly into a liquid bath. Fine materials can therefore be charged without the need for agglomeration. Milling and agglomeration steps can be saved, including costs for installation, maintenance, and operation of the required equipment.

Production of FeCr in DC furnaces is practiced in South Africa and Kazakhstan. In South Africa charge chrome (ChFeCr) is produced and in Kazakhstan high carbon ferrochrome (HCFeCr). This paper focuses on the production of HCFeCr in using a Kazakh ore, known for a high Cr:Fe ratio and a high MgO content.

The Kazakh and South African DC furnaces operate well today, but experienced slow start-ups.[3,4] At least some of the issues in the early years of operation can be related to not fully understanding the processes within the furnace that affect operation.

This paper aims to increase understanding of process mechanisms in a DC FeCr furnace, taking the Kazakh FeCr furnaces as a case-study. Improved understanding of mechanisms inside a DC furnace can help considerably to support smoother start-up, (safer) up-scaling and load increase, improved operation, and reduction of environmental footprint. Observations and conclusions may be applicable to other open-bath operations, of which FeCr, TiO_2-slag, and processing of iron units are the most relevant at the moment.

Better process understanding can be achieved by studying average conditions and thermochemical equilibria in discrete zones inside the furnace. Gleaning from industrial experience, various zones have been identified as discrete, important sub-reactors within the furnace.

This paper reports on a theoretical analysis of possible reactions in the high temperature zone under the electrode in DC furnaces that process Kazakh chrome ore. The focus is on reaction products that form, and specifically the role of fuming in the associated energy transfer and exergy dissipation from the arc-zone.

To improve understanding of reaction mechanisms in this zone, two scenarios were studied with FactSage[5] equilibrium calculations by varying temperature, carbon-to-Cr_2O_3 ratio, and slag-to-feed ratio. This was then interpreted in relationship to industrial furnaces to better understand energy consumption and exergy dissipation. In summary, this paper reveals some important mechanisms in the AAV zone and relates the findings uniquely to industrial scale operation, shedding significant light on energy consumption in DC arc furnaces for HCFeCr and also for the first time sheds light on exergy flows around the AAV. For clarification, a cross-section of a DC furnace is given in Fig. 1, with a close-up and explanation of the AAV in Fig. 2.

II. TECHNICAL BACKGROUND

This section provides an overview of DC FeCr smelting operations in Kazakhstan with a focus on process control. Some data on South African operations is given to indicate both relevance to and differences with the Kazakh operation. Especially a visualization of the principal zones in the furnace is provided, gleaned from industrial experience in the operation and commissioning of such furnaces. This is followed by a brief introduction to metallurgical calculations, and how these relate to a multi-zone model. Finally, it is explained why focusing on a single zone—in this case the arcing zone—is a meaningful approach to better insight in the process mechanisms of a DC FeCr furnace.

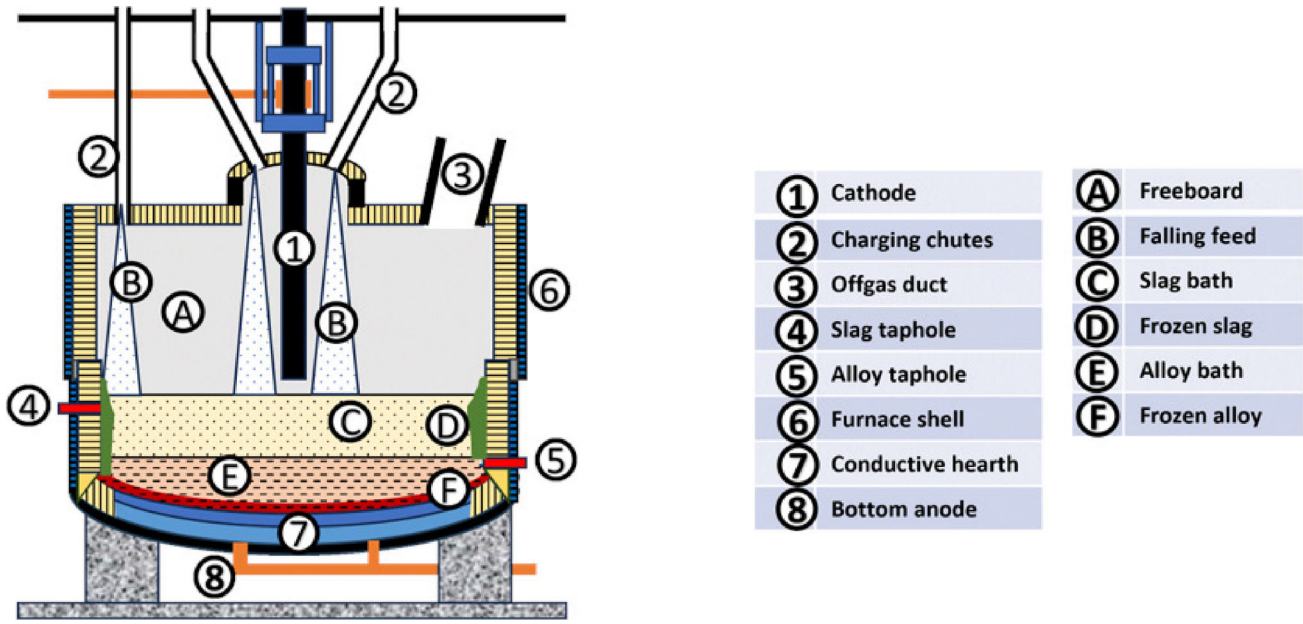

Fig. 1—Schematic cross-section of a DC furnace. Based on information from[12–14] the electrode is 750 mm and the furnace has an approximate diameter of 13.5 m. Not shown are furnace bins and continuous feeders.

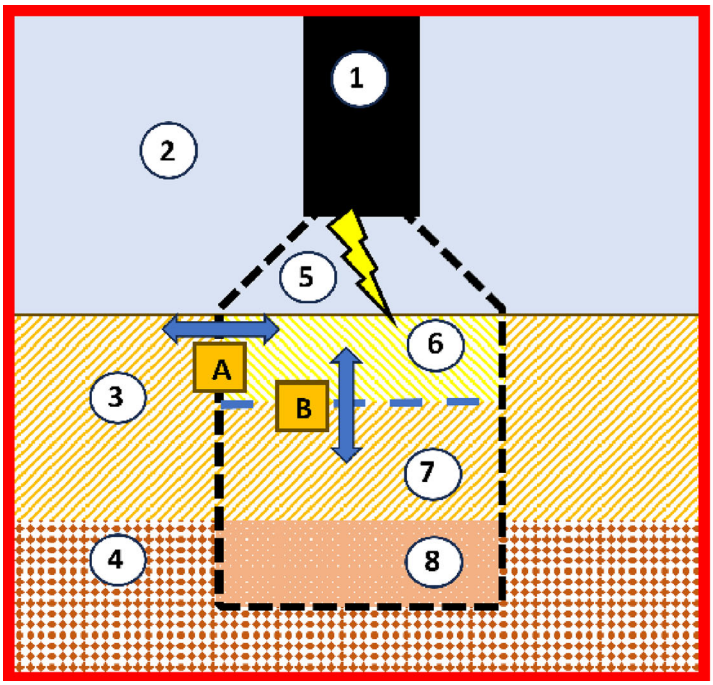

Nr	Description
A	AAV boundary 1 with variable diameter
B	AAV boundary 2 with variable level
1	Electrode
2	Furnace freeboard
3	Bulk slag bath – not part in AAV
4	Bulk alloy bath – not included
5	AAV: plasma and process gas - included
6	AAV: slag bath - included
7	AAV: slag bath – not included
8	AAV: alloy bath – not included

Fig. 2—Sketch of the AAV. Note that the diameter of the AAV is variable as well as the height of involved bath, which could extend down to include alloy. In the given example in figure 2 only the top layer(6) of the slag is included in the AAV, while the lower slag volume and the alloy volume are not included in the AAV. By extending B downward, the AAV can be enlarged to even include alloy bath.

A. *Chromite Smelting in Kazakh and South African DC Furnaces*

Raw materials for the production of FeCr in a DC furnace are chromite ore, reductants like coke or anthracite, and fluxes like quartzite, bauxite, magnesite, dolomite and limestone.

Some available data on the Kazakh and South African operations are given in Table I.

Note specifically the differences in the compositions of ore from South Africa and Kazakhstan. These lead to different alloy and slag compositions and subsequently different tapping temperatures for alloy and slag.

Feed materials are dried before or after being transported into storage bunkers for further use. Drying to a fixed, low value is important because this saves energy, reduces variability in energy and carbon consumption, and thereby stabilizes the feed-to-power ratio and the carbon addition required. The basic reactions in DC FeCr smelting are given below.

The main equation of the complete reduction of Fe and Cr in chromite ore to carbide is given by Eq. [1]:

$$(\mathrm{Fe,Mg})\mathrm{O}\cdot(\mathrm{Al,Fe,Cr})_2\mathrm{O}_3(\mathrm{s}) + \mathrm{C(s)} = (\mathrm{Cr,Fe,C})(\mathrm{l}) + \mathrm{CO(g)} + (\mathrm{MgO}, \mathrm{Al_2O_3}, \mathrm{SiO_2})(\mathrm{l}) \quad [1]$$

No numbers are given for stoichiometry in Eq. [1] because of the undefined formula for chromite. In the production of HC FeCr, carbon is mainly used for:

- reduction of chromium oxides,
- reduction of iron oxides, and
- formation of carbides.

The simplified formula for the reduction of Cr_2O_3 is given in Eqs. [2] and [3]:

$$x\mathrm{Cr_2O_3(l)} + (2y+3x)\mathrm{C(s)} = 2\mathrm{Cr}_x\mathrm{C}_y(\mathrm{l}) + 3x\mathrm{CO(g)} \quad [2]$$

$$3\mathrm{Fe}x\mathrm{O}y(\mathrm{l}) + (3y+x)C(\mathrm{s}) = x\mathrm{Fe_3C(l)} + 3y\mathrm{CO(g)} \quad [3]$$

The important reaction representing the pre-reduction of Cr_2O_3 is given in Eq. [4]:

$$\mathrm{Cr_2O_3(l)} + \mathrm{C(s)} = 2\mathrm{CrO(l)} + \mathrm{CO(g)} \quad [4]$$

Relevant side reactions include:

$$\mathrm{SiO_2(l)} + 2\mathrm{C(s)} = \mathrm{Si(l)} + 2\mathrm{CO(g)} \quad [5]$$

$$\mathrm{SiO_2(l)} + \mathrm{C(s)} = \mathrm{SiO(g)} + \mathrm{CO(g)} \quad [6]$$

$$\mathrm{MgO(l)} + \mathrm{C(s)} = \mathrm{Mg(g)} + \mathrm{CO(g)} \quad [7]$$

$$\mathrm{Cr_2O_3(l)} + 3\mathrm{C(s)} = \mathrm{Cr(g)} + 3\mathrm{CO(g)} \quad [8]$$

$$\mathrm{FeO(l)} + \mathrm{C(s)} = \mathrm{Fe(g)} + \mathrm{CO(g)} \quad [9]$$

These reactions are unwanted as they consume energy, but can happen if temperature, oxygen potential, and activities allow so.

Finally, there are the Boudouard reaction and reactions involving water:

$$\mathrm{CO_2(g)} + \mathrm{C(s)} = 2\mathrm{CO(g)} \quad [10]$$

$$\mathrm{H_2O(g)} + \mathrm{C(s)} = \mathrm{CO(g)} + \mathrm{H_2(g)} \quad [11]$$

Table I. Comparison of Kazakh and South African DC Ferrochrome Operations

		Kazakhstan		South Africa	
Ore	Unit	[6]	[7]	[6]	[8]
Cr_2O_3	pct	51.2	52.3	42.9	43.5
FeO	pct	11.9		28.5	25.2
Fe_2O_3	pct		13.9		
SiO_2	pct	6.9	6.6	3.0	4.0
MgO	pct	19.8	19.9	8.8	10.0
Al_2O_3	pct	6.5	6.7	15.7	14.5
CaO	pct	0.2–0.3	0.11		0.5
Cr:Fe Ratio	—	3.8	3.8	1.4	1.5
Slag	Unit	[6]	[9]	[10]	[8][a]
Cr_2O_3	pct	6.0	3.9		
FeO	pct	1.4			
SiO_2	pct	28.1	21.8		26.0/28.0
MgO	pct	42.7	44.2		22.0/23.0
Al_2O_3	pct	18.6	24.5		34.0/35.0
CaO	pct	0.7	0.55		18.0/14.0
Liquidus Temp.	°C				
Tapping Temp.	°C	1828	1800	1650	1620–1640
Alloy	Unit	[6]	[11]	[10]	[8]
Cr	pct	71.0	71.0	53	53.5/52.0
Fe	pct	18.7	20.0	40.5	
Si	pct	0.17	1.0	0.5	1.0/4.0
C	pct	7.8	8.0	8.0	8.5/7.5
Liquidus Temp.	°C		1644		
Tapping Temp.	°C	1800	1700	1570	1550
Other	Unit		[4]		
Energy/t Alloy	kWh		4500–4700		

[a]Normalized slag composition excluding Cr_2O_3 and Fe..

$$H_2O(g) + CO(g) = CO_2(g) + H_2(g) \quad [12]$$

$$O_2(g) + 2C(s) = 2CO(g) \quad [13]$$

These reactions play an important role in the formation of hydrogen and keeping the oxygen potential low.

When raw materials are needed in the furnace bins, the desired mix is prepared by a batching system according to set-points dictated by operational conditions. One of the two most important parameters for process control is the mass of added carbon relative to the mass of reducible oxides in the total feed mix, as this controls the degree of reduction of the oxides and therefore a large part of the energy consumption. The other important ratio, feed-to-power, is explained shortly. All reducible oxides do not only include FeO and Fe_2O_3, but also oxides like MgO and SiO_2.

In this paper, the ratio of charged mass of fixed carbon to the charged mass of Cr_2O_3 is used, and is called the carbon ratio (RC, to prevent confusion with Cr, chromium). It only considers Cr_2O_3 because Cr_2O_3 is the main consumer of C and this ratio allows for clear communication regarding the recipe even when there is a change in composition of ore or reductant. The RC is mostly determined by the carbon needed for carbide formation, as given in Eq. [2].

$$RC(kg/kg) = \frac{\text{Feed rate of fixed carbon}}{\text{Feed rate of } Cr_2O_3}\left(\frac{kg/h}{kg/h}\right) \quad [14]$$

The remainder of the RC mostly comes from the side reactions given in Eqs. [4] through [11]. The RC is used as an industrial and rough proxy for the mentioned reactions to make decisions regarding the recipe for the feed mix. However, this practical RC does not often provide the detail to fully operate the furnace at minimum energy consumption.

Having made this "rough" estimate for the RC, batches of pre-mixed raw materials are then charged into the furnace bins. From these bins the feed mix is extracted continuously with screw conveyors and falls *via* center or sidewall chutes through the freeboard into the slag bath. These chutes are shown in Figure 1.

Charged feed is smelted by discharged electrical energy, which in normal operation is released (1) mostly by an arc in the small volume between the cathode tip and slag bath acting as anode, and (2) to a limited extent by Joule heating in the slag bath.

The area where the arc connects to the slag bath, being the anode, is called the arc attachment zone (AAZ). The volume between cathode and AAZ and extending into the bath is referred to as the arc attachment volume (AAV) in this paper (Fig. 2).

The AAV is shaped like a dome or capped cone above the AAZ and like a cylinder below the AAZ. Note that the AAZ is only a plane within the AAV and that the AAV can include both slag and alloy.

This paper refers to the AAZ being the surface where the arc connects to the slag bath. AAV is used for the reaction volume where feed, slag, and alloy react under influence of the arc. In the arc and AAV, temperatures can be well above slag tapping temperature of 1800 °C, therefore reactions can take place here that are different than if one considers only slag tapping temperatures.

The slag bath is connected to the bottom anode *via* the alloy bath and electrically conductive hearth refractory.

To distribute feed as evenly as possible, multiple chutes are installed concentrically in the furnace roof. Typically, a ring of chutes is present close to the electrode and some chutes are installed at the periphery, as shown in Figure 1.

The other of the two most important parameters to operate such a furnace is the feed-to-power ratio (FTPR). This is the ratio between the mass of feed mix charged and electrical energy input during a certain time interval.

$$FTPR(kg/kWh) = \frac{\text{Feed rate}}{\text{Power input}}\left(\frac{kg/h}{kWh\ /h}\right) \quad [15]$$

The electrical energy input needed for any feed rate is the sum of energy required for smelting the feed mix to reach the targeted production and for compensating thermal losses of the furnace. One of the reasons why

the FTPR will vary with different power set-points is that the relation between furnace load and thermal losses is typically not linear. Another is that the furnace condition, for example refractory wear, also affects the FTPR. This makes the FTPR a difficult parameter to manage, because it must be manually set by the operator based on calculations and observations. Barcza[15] argued that a deviation of 0.5 pct between power input and feed rate could already prove problematic. Therefore, a loss-in-weight system is installed to accurately measure material charged into a furnace.

To date, feed material is charged into the Kazakh FeCr DC furnaces at ambient temperature, but preheating and pre-reduction are possible. The main reason for applying cold charging is that preheating (and pre-reduction) of feed can introduce variability in its temperature and composition. That variability affects the energy required to smelt the feed, which affects the FTPR and that makes stable operation of the furnace harder.

As slag and alloy are formed, alloy sinks through the slag bath into the alloy bath due to its higher density. In the Kazakh case, slag and alloy are tapped from different levels at regular intervals. Slag is tapped at about 1800 °C, while alloy is under normal conditions tapped at about 1700 °C.

Frozen layers of slag and alloy are desirable for protection of furnace sidewalls and hearth. Gases, fumes, and dust leave the furnace through the stack.

B. *Calculating Mass and Energy Balances for DC FeCr Smelting*

This section explains the basic form of calculating a mass and energy balance for a DC FeCr smelting operation. The results can be used to determine the RC and FTPR, but this method does have limitations which are also explained. Subsequently, an alternative method is described which relates to the title of this paper, which is of value to industrial practice.

1. *Limitations of basic mass and energy balance models*

The simplest form of a mass and energy balance for a furnace only considers input and output streams, without any consideration for reactions taking place inside the furnace. Such a calculation can be referred to as a one-step black-box calculation. The required material streams for a one-step black-box approach are shown in Figure 3.

The steady-state mass- and energy balance for the process, also to estimate the RC and FTPR, can be calculated with the following information:

1. quantity, composition, and temperature of feed materials going into the furnace,
2. quantity, composition, and temperature of alloy, slag, gas, and dust leaving the furnace, and
3. heat losses.

Calculated product compositions can be based on experimental distribution factors or thermochemical calculations based on equilibrium Gibbs free energy computations. Energy requirement for the process is calculated in a single step as the difference in enthalpy between output and input materials, as is normal in industrial practice. Thus, the reactor is considered a black-box without including and revealing the intricacies within and between zones within the reactor, especially not the AAV. The one-step methodology is limited and does not reveal and divulge an understanding of what mechanisms occur within the furnace regarding how, where, and why the overall process is affected by changes in feed, power input, and quantity and direction of heat and mass transfer. Finally, the one-step black-box approach does not allow investigation of reaction steps that happen inside the process. Therefore, to develop a deeper understanding, the process needs to be split into multiple processing zones that interact with each other: a multi-zone model.

2. *Multi-zone modeling of a DC FeCr furnace*

The concept of multi-zone modeling in pyrometallurgy is not new. Numerous papers on processes and furnaces with different types of multi-zone models have been published.[16–24] Ideally a model combining computational fluid dynamics and thermochemistry should be used to simulate the entire furnace at once, but this is still very complex and computationally expensive. A way to simplify such a simulation is by selecting a limited number of zones that have distinct features. The more zones used, the more model parameters must be specified, which increases complexity. The number of zones is therefore typically kept to those considered most relevant for the situation being studied.

From industrial experience, zones were selected based on criteria like temperature, density, volume, or the phases present, for example:

1. the slag and alloy baths contain very different materials with different temperatures, densities and compositions, and
2. the freeboard contains gases, dust, and falling feed which have very different properties compared to the bath zones, and may again be divided into:
   (a) an area where oxidic feed enters at ambient temperature, which locally lowers temperature and raises oxygen potential,
   (b) a region where mechanical dust is transported by evolving gases towards the stack, possibly reacting during the transport, and
   (c) the rest of the freeboard where falling feed can interact with evolving process gases and fumes.

It is self-evident that a DC furnace with a load over 40 MW is not a perfectly mixed reactor at a single temperature, but contains a multitude of variations of solids, gases, liquids, and plasma, each at a range of temperatures and compositions. These materials move through the furnace, in possibly a stochastic way, and interact and react with each other driven by laws of physics and thermodynamics.

Reactions towards equilibrium will start depending on temperature, partial oxygen pressure, and materials present in a certain zone, while the residence time, state, and size of the materials determine how far reactions go. Once conditions change, equilibria will also shift.

Because of the range in temperatures, residence times, and properties of materials inside a DC furnace, it is unrealistic to assume all products are formed at a single temperature. The integral effect of all reactions in the different reaction zones inside the furnace balance towards a process state that is observed through analyses and measurements of slag, alloy, dust, and off-gas.

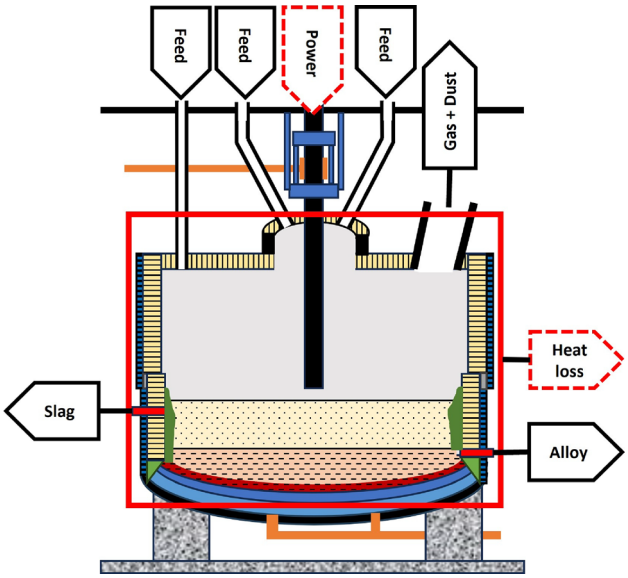

Fig. 3—Schematic view of a black-box model where only information for the input and output streams is considered.

Thus, as an alternative to the modeling approach in Figure 3, a DC FeCr smelting process can be described as shown in Figure 4. The model is divided into nine zones, derived from industrial experience, represented by the nine circles. These zones should not be seen as static areas located there where each circle is depicted. The zones will change shape and volume due to charging, splashing, tapping, eruptions, and other changes affecting and involving heat and mass transfer. Each zone therefore represents a conceptual reaction volume whose physical size can vary, but where the temperature is set for that volume, and material and heat can flow in and out.

The zoning of the furnace in such a manner helps to better understand the effect of multiple interactions that describe the process. In summary, it is postulated that for the understanding of the furnace the integral of the mechanisms within the furnace is simplified sufficiently by these zones to limit the computational burden to something that is manageable but also revealing of mechanisms and interactions between the zones.

3. *Focus on a single zone*

By dividing the furnace into multiple zones, it is possible to investigate each zone individually. This creates insight into the products that could come out of each zone, and how the transport of material and energy could affect other zones and the overall process.

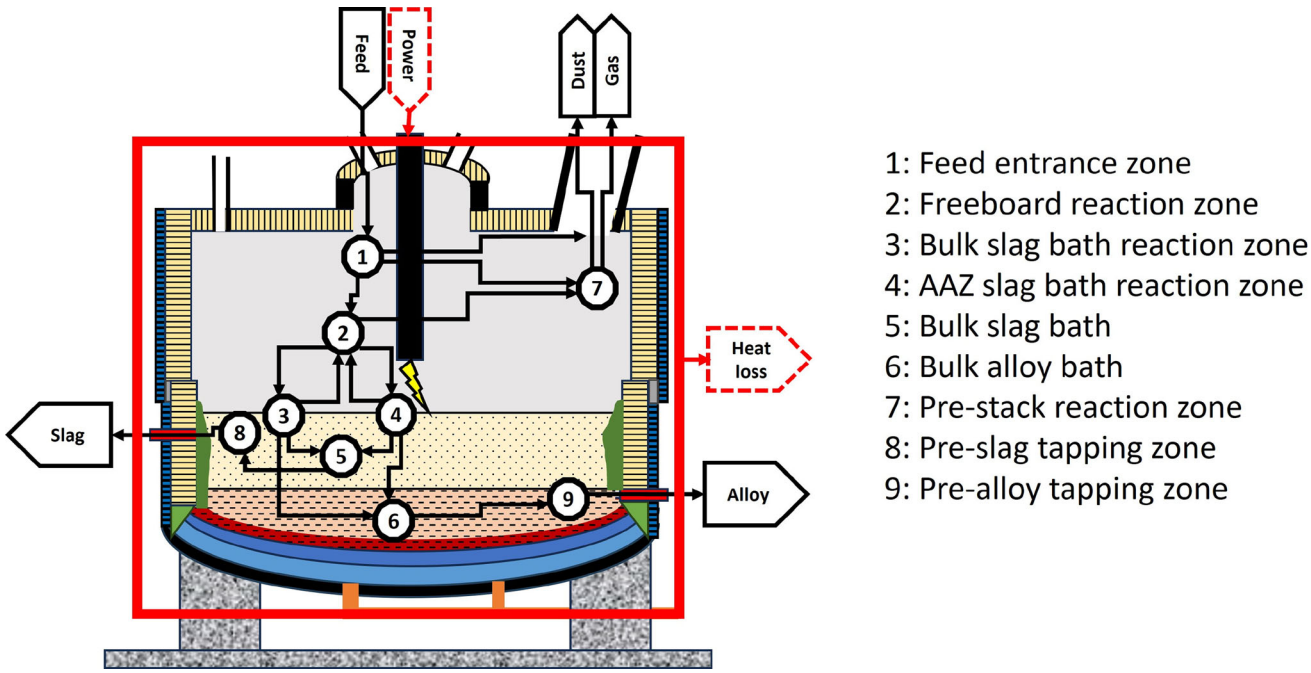

Fig. 4—Schematic view of a multi-zone model for FeCr DC smelting with interaction between falling feed and process gases in zone 2, and separate reaction zones for smelting feed material near the electrode (4) or further away (3).

The area of interest in this paper is the AAV, marked by (4) in Figure 4, and as will be shown has great significance. Temperatures are and can be significantly higher in this zone than the normal average operating temperatures measured for slag and alloy at the tap holes, or for process gas and dust in the stack. The high temperatures create conditions under which reactions take place that are thus far beyond the normal operating conditions and therefore may affect the process in a manner not captured by normal temperature conditions using a black-box approach. An awareness, therefore, of the products that form under the cathode and the interactions of the reaction products with other zones, is useful for better understanding of the entire smelting process. Consequently, the results from the investigation of the AAV are also useful when analyzing the reaction mechanisms in connected zones. Examples of such zones are the freeboard and slag bath, where the materials present can interact with the reaction products formed during the very high temperature processes in the AAV.

III. LITERATURE REVIEW

This section reviews literature related to reactions in the AAV. The following aspects were reviewed:

1. open-bath smelting of FeCr,
2. SAF burden smelting of FeCr,
3. open-bath smelting of other processes than FeCr, and
4. material falling through an arc.

In summary, plenty of literature can be found that AC and DC arc furnaces have been used to smelt chromite, but very little is published on reactions taking place in the hottest zone directly under the electrode. Fuming has been reported on slags containing MgO and SiO_2 but a quantification of the fuming was found only in carbothermic magnesium production.

A. *Open-Bath FeCr Smelting*

In 1935 Koster, Shelter, and Knickerbocker[25] did tests for the US Bureau of Mines on domestic chromite in a 35 kVA induction furnace. From a slag bath "puffs of white fume" were used as an indicator for the progress of reactions, but no analysis of the fume was given.

In 1950 Wessel and Rasmussen described small-scale open-bath FeCr smelting tests at around 70 kW in which an SiO_2-rich slag was used.[26] In these tests, observing formation of "flaky particles of fume" was used for process control. Analyses of fume samples showed the fume consisted mainly of SiO_2 and MgO. Alloy composition varied based on carbon addition and "to some extent by the power input".

Taneka and Robertson[27] used a lab-scale DC furnace for the reduction of Zimbabwean chromite, which is quite similar to Kazakh chromite. They concluded based on analyses of dust and accretions that fuming of MgO and SiO_2 took place, especially when abundant reductants were available.

In 1990 Barcza[15] used Pyrosim[28] to evaluate a system with equal masses of CaO, SiO_2, MgO, and Al_2O_3, with an additional 10 pct of Cr_2O_3 and 1.0 pct of FeO. Temperature was taken in the range from 1650 °C to 2500 °C and carbon added from 1.0 to 15 pct relative to the mass of the slag excluding the Cr_2O_3 and FeO. Calculations showed that with increasing temperature the reduction of MgO and SiO_2 to Mg and SiO gas is more favorable than reduction of iron and chromium oxides. It was not mentioned that C and Cr can act as reductants for slag. The authors did not consider possible consequences of the formed gases on the FeCr smelting process.

Eksteen[29] applied data reconciliation to a DC FeCr furnace and concluded that tapped slag and alloy are not as homogeneous as expected and that analyzing dust is important. Dust analyses showed enrichment in Si and Mg, as well as presence of "tiny specks of metal entrained in dust".

The formation of Cr^{6+} smelting of chromite ore in a 300kW DC furnace was investigated by Berryman.[30,31] Though fuming of slag components was mentioned, no in-depth investigation on the fume was done. It is suggested that the formed fumes play a role in Cr^{6+} formation, but without thermochemical calculations to support this.

From the above it is clear that fuming of MgO and SiO_2 takes place in DC FeCr smelting, but no paper quantifies it or its potential role. Though[15] showed that alloy may under these conditions become a reductant, none of the other papers observed this mechanism during their small-scale experiments.

B. *Reactions in SAF FeCr Production*

Bowman[32] describes extensively what can happen at the electrode tips in a FeCr SAF. Relevant aspects for this paper are for example that plasma is present with temperatures probably up to 10,000 °C, that radiation effects are important, and that the slag present provides input to the plasma composition. He also commented that "...there is a strong likelihood that the slag surface is boiling, but to an unknown extent". Some possible reactions have been described previously in Section II–A. No comments in[32] were made regarding alloy.

One test described in[33] was on producing FeCr-silicon, a FeCr alloy with significant masses of silicon and even aluminum. Adding large quantities of reductant to a pilot-scale furnace resulted in reduction of "other oxides present in the chromite", formation of "voluminous quantities of fumes", and "very little slag". An inverse correlation between Si and C was observed.

That carbon in alloy can reduce Cr-oxides in slag has been reported by several investigators, for example.[34–36] On an industrial level little relevant information is found. Volkert *et al.*[37] state that in an SAF burden operation the carbon content in alloy can be reduced by increasing temperature and the reactions taking place between carbon in the alloy and available Cr_2O_3.

These publications confirm that the behavior of slag and the addition of carbon in high temperature calculations is important and reduction of ore by carbon in alloy can take place. No references for industrial SAF smelting were found where very high temperatures cause chromium to become a reductant.

C. *Formation of SiO(g) and Mg(g) Fumes in Other Open-Bath Processes*

Billiton Research[38] used a 200 kW arc furnace equipped with graphite electrodes to fume Mg with carbon from an $MgO–Al_2O_3–CaO$ slag bath with only 25 pct MgO. Good fuming was achieved at temperatures above 1750 °C.

Mintek developed a DC smelting process for the production of magnesium metal in which dolomite is smelted together with FeSi in an open-bath.[39] A key feature is that Mg is deliberately fumed out of the slag bath with about 20 pct MgO. Though the reductant used is FeSi, the operating temperature is only 1700 °C to 1750 °C, which is below that used in the Kazakh DC FeCr operation. In the conditions described, 63 to 87 pct of magnesium charged as dolime (MgO–CaO) was fused as gaseous magnesium and recovered in an external condenser as magnesium metal.

Two types of dust—called "dust" and "fume" by the authors—from titania slag production were investigated for cementitious properties[40] in a joint French-Canadian project, implying the material came from the open-bath 6-in-line Rio Tinto ilmenite smelters. The formation of the vitreous fume was explained by generation of vapors due to temperatures over 1700 °C in the arc-zone of the electrodes. The ilmenite "fumes" were analyzed, and the small particle size distribution together with the round shapes clearly pointed to condensation.

Dust from a South African DC ilmenite smelter was investigated by Rughubir and Bessinger.[41] A careful conclusion was drawn that fuming of SiO_2 and MnO led to the enrichment of both in the furnace dust. In 2016 dust from the same smelter was investigated by Khesa.[42] Composition, particle size distribution, and shape pointed again to condensed gases, but no explanation on formation was given other than that given in the papers on ilmenite already mentioned.

To summarize, in magnesium production, Mg is fumed from slags as low as 20 pct in MgO and around 1750 °C. This implies that high Mg fuming rates can be reached when smelting Kazakh ore with over 40 pct MgO in the slag and temperatures over 1800 °C.

D. *Ore Falling Through an Arc into the Bath*

Oxide ore falling through the arc, which is part of the AAV, has been investigated in the past, and is currently of interest again primarily for iron ore,[43–45] but also for chromite.[46] When chutes are positioned close to the electrode, then feed material may (partially) fall through the AAV or even through the arc.

The in-flight plasma and sustained shock-wave reactor (SSR) at the University of Minnesota, falling film reactor at Bethlehem Steel, extended arc flash reactor (EAFR) at the University of Toronto all processed chromite in some sort of laboratory-scale DC furnace. Little attention, excepting small comments, was given to fuming.

The SSR tests by Moore and others did not find any reduction of MgO or Al_2O_3, while SiO_2 was not even mentioned, but did record nearly 50 pct of FeO reduction and between 5 and 10 pct of Cr_2O_3 reduction even when residence time was less than 100 ms.[47]. A "white fluffy material" on the cathode was found to be MnO. Some sodium and chromite were also volatilized, though no more details were given, and the composition of the charged chromite is unknown.

Tests at Bethlehem Steel produced low-carbon FeCr with a low Cr recovery, but further tests were canceled.[48] Nothing was found on fuming of components.

Concerning the EAFR, Sommerville *et al.*[49] suggest that sulfur is removed from the slag as SiS(g). Formation of SiS(g) could be confused with formation of SiO(g), because both end up as SiO_2 when interacting with oxygen or water. The same paper states that "...some... partial melting and reduction occur during the free fall of the particles counter-current to the hot reducing gases leaving the plasma zone", but without specifying the composition of the gases.

In the small in-arc test facilities again little attention was given to fuming, but in some tests sulfide fumes were reported. On an industrial scale ilmenite is charged through hollow electrodes. Enrichment of certain components in the dust of ilmenite smelting may have been observed, but it cannot be concluded this happened because of the hollow electrode, or not.

IV. ANALYTICAL APPROACH TO UNDERSTAND THE THERMOCHEMICAL PHENOMENA IN THE AAV

Reactions in the AAV were investigated with FactSage (7.2) calculations, using the databases FactPS, FToxid, and SGTEa. In two scenarios thermochemical equilibrium of a mass of ore, carbon, and fluxes is calculated, with a focus on the reactions described in Section II–A. Details for these scenarios are given in Table II.

A. *Scenario 1: Effect of Carbon and Temperature*

In this scenario, the thermochemical equilibrium is calculated for the basic mix given in Table III, while varying the RC and the equilibrium temperature as given in Table II.

Temperature is increased in steps of 25 °C to have small enough steps without overloading FactSage. The RC in the feed mix is increased in steps of 2 pct from 12 pct below to 12 pct above the actually required quantity of carbon (RC = 0 pct) that is given in Table III.

Table II. Description of the Two Scenarios Investigated

Scenario	Ore Feed Rate Tonne/Hour	Temperature Range °C	Carbon Ratio (RC) kg/kg	Slag to Feed Ratio kg/kg
1	20.0	1650–2500	0.363–0.461[a]	0
2	20.0	1650–2500	0.412	0–10

[a]The RC is given as a value ranging from −12 to +12 pct.
0 pct equals 0.412, which is the RC for the basic feed mix used in this paper.

Table III. Feed Materials Used in the Calculations

	Unit	Ore	Bauxite	Quartz	Reductant	Sum
Feed Rate as Received	t/h	20.00	1.00	0.20	5.00	26.20
Free Moisture	pct	2.0	2.0	2.0	2.0	2.0
Free Moisture	t/h	0.39	0.02	0.00	0.10	0.52
Volatile Matter	pct				3.0	
Temperature	°C	25	25	25	25	25
		Pct	Pct	Pct	Pct	kg/h
Cr_2O_3		50.0				9800
FeO		12.5				2450
Fe_2O_3		0.0			2.0	95
SiO_2		7.0	10.5	100	7.0	2003
MgO		20.5			1.5	4089
Al_2O_3		8.5			4.0	1856
CaO		0.5			0.50	121
C					85.0	4038
LOI H_2O		1.0				196
$Al(OH)_3$			76.0			745
$Fe(OH)_3$			12.0			118
TiO_2			1.5			15
Sum (Air Dry)		100	100	100	100	25, 688[a]
Sum (as Received)						26,203

[a]Includes 162 kg volatile matter (122 kg CH_4(g) and 40 kg N_2(g)) from reductant
The carbon ratio (RC) is given by the ratio of C to Cr_2O_3, 0.412 in this case

The range is selected based on the idea that fluctuation in the RC of the charged feed material can be caused by variation in for example:

- Cr_2O_3 content of ore from 48 to 52 pct,
- C content of reductant from 82 to 88 pct, and
- moisture content of ore or reductant from 1 to 3 pct.

When certain variations in the feed materials occur simultaneously, then a deviation of 12 pct is possible. Additionally, it may sometimes be considered in FeCr production to deliberately change the RC when for example the composition of alloy or slag is out of spec. Investigating a broad RC range supports understanding of potentially unintended consequences of a recipe change.

B. *Scenario 2: Effect of Slag and Temperature*

In this scenario the thermochemical equilibrium is calculated for the basic mix given in Table III while including an increasing mass of slag from the slag bath and varying the equilibrium temperature as given in Table II.

The ratio of slag mass to feed mix mass is given as Alpha in kg/kg.

$$\text{Alpha}(\text{kg/kg}) = \frac{\text{Mass of slag from the slag bath at } 1800\,^{\circ}\text{C}}{\text{Mass of feed mix at ambient temperature}} \left(\frac{\text{kg}}{\text{kg}}\right) \quad [16]$$

This calculation is done to gain insight on the effect of slag mass and temperature on the equilibrium composition.

The slag used in all calculations has a temperature of 1800 °C and the composition is given in Table IV.

A range of 0 to 10 was selected for Alpha over a temperature range from 1650 °C to 2500 °C.

Investigating the slag-to-feed ratio is interesting because:

- It seems plausible that (part of the) feed will mix with slag from the slag bath, and this mixture reaches an equilibrium.
- As the furnace load is increased, the feed rate must be increased to maintain the FTPR, but the slag bath surface where the feed falls will not change much: this results in variation in the slag-to-feed ratios.

Table IV. Slag Used in Scenario 2

Temperature	1800	°C
Moisture	0	Pct
Cr_2O_3	5.0	pct
FeO	1.5	pct
SiO_2	22	pct
MgO	45	pct
Al_2O_3	26	pct
CaO	0.5	pct
Sum	100	pct

By comparing the feed rate and the possible mass of slag available in the zone where feed falls over a certain time step, it is possible to estimate if slag can affect the equilibrium in an open-bath DC furnace. For the DC FeCr furnace as constructed in Kazakhstan following comments can be made regarding the slag available:

- Taking a hearth diameter of approximately 13.5 m and a slag bath of 1.0 m depth, the furnace contains a mass of approximately 400t to 450t of slag.
- A feed rate of 26 tonne/h equals about 430 kg/min, or 7 kg/s.
- The volume of slag in a 1.5 m radius around the electrode is approximately 7 cubic meters, which is equivalent to about 20 metric tons.
- When considering a layer of slag with a 500 mm radius and depth of 100 mm for the AAV, then 60 kg of slag is present which can be very dominant in the equilibrium that establishes near the electrode each second.

Concluding, with the likely fast reaction kinetics in the AAV due to temperature, turbulence, and feed particle sizing,[50] and the small charging rate per second compared to the mass of slag present in even a small AAV, the slag-to-feed ratio may well be a relevant aspect in understanding the DC FeCr smelting process better.

For this scenario, the following simplifying assumptions are made:

- reactions are very fast due to the turbulence and high temperature near the arc,
- mixing is intense and the AAV interacts with the bulk of the slag bath keeping the reacting slag composition constant,
- slag-to-feed ratios between 1 and 2, and bigger than 10 are not investigated, and
- all feed flows into the AAV.

Note that in one minute 430 kg of feed mix is charged. An Alpha of 10 means that 4.3 metric tons of slag takes part in an equilibrium reaction. That mass of slag is already available in a slag volume of:

- 1 m depth and a radius of 0.8 m, or
- 0.25 m depth and a radius of 1.6 m.

C. *Model Configuration for Both Scenarios*

A calculation for an operation of 1 hour at a setpoint of 40 MW was done using information from Table I and[4] to have an estimate of the feed mix composition, the C:Cr_2O_3 ratio (RC), and the feed rate. Published data are used to select the composition for a representative realistic ore. Reductants and fluxes are simplified.

The conceptual basis that is applied to model the phenomena is depicted by Figure 5.

As explained, the AAV is the 3-dimensional volume under the electrode expanding into the slag bath and even alloy bath, if alloy is to be considered in investigations: width and depth of the AAV are variable. The AAZ is part of the AAV. It is the objective to use this model for both scenarios to establish and understand what happens in the AAV especially regarding:

- the quantity and composition of formed reaction products,
- the energy balance,
- exergy flow and efficiency,
- energy that can be transported by formed reaction products, and
- the range of partial oxygen pressures.

D. *Used Materials*

Data in the following tables are based on publicly available data, as tabulated in Table I, and do not represent operational data. Table III summarizes the raw materials used in the calculations. Table IV provides the slag composition that is used in scenario 2.

E. *Simplifications and Assumptions*

For both scenarios some simplifying assumptions were made:

- As discussed previously, the RC is a simplified way to control and report reductant addition to the feed mix without having to be too concerned about other reducible oxides (mainly Fe*x*O*y*, MgO, SiO_2, H_2O). Industrially, any other factor affecting carbon consumption would also need continuous manual adjustment of the RC. Constant monitoring of the mass balance data are a requirement because of the creation of volatile compounds that are fumed such as Mg(g) and SiO(g), as well as C and Si content of the alloy. Not to be forgotten is the effect of moisture in the feed.
- Pressure is set to 1 atmosphere for all calculations, even those taking place within the bath where a certain pressure may affect for example the reactions creating volatile species.
- The investigated temperature range is 1650 °C to 2500 °C. This obviously does not consider all temperatures possible in a plasma arc.
  - The lower limit of 1650 °C was chosen to exclude some interesting yet distracting equilibria compositions.

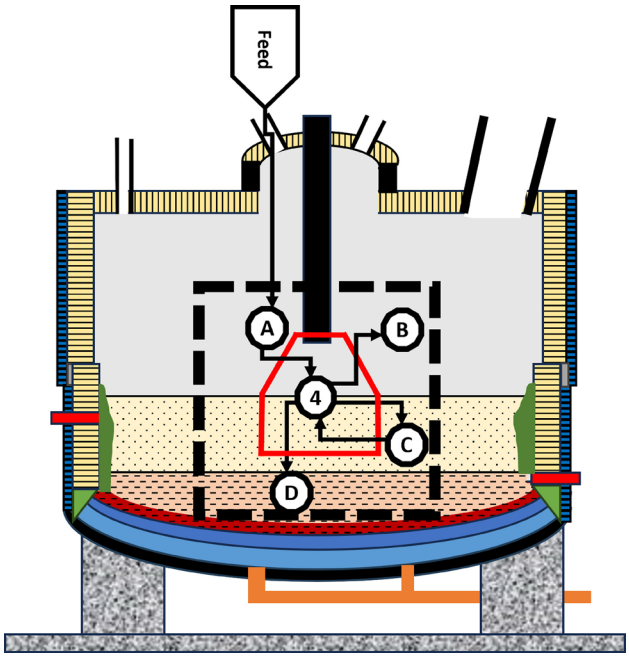

Fig. 5—Schematic view of the arc attachment volume (AAV) depicted in red under the electrode inside the dashed box, where (*A*) represents the feed material input stream, (4) the AAV slag bath reaction zone, (*B*) the fumes and process gasses that are formed, (*C*) the slag that is formed including a stream of slag that can participate in the equilibrium calculations, and (*D*) the alloy that is formed (Color figure online).

  - The upper limit of 2500 °C was chosen because at this temperature no alloy is present anymore with the given input, as it is all volatilized.

- All input materials are to some extent simplified by rounding off or by ignoring components such as S and P, or a detailed analysis of volatile matter in reductants.
- The absence of S also means that no fuming of sulfides such as SiS(g) can take place.
- This investigation considers thermochemical equilibrium of the entire AAV and assumes perfect mixing; while mixing under the electrode will be intense, it is probably not perfect as is usual at industrial scale, implying that there may be strong variation in temperature or composition on very small distances.
- The composition of the slag in the AAV may not be the same as tapped slag, but will be the result of many factors, including strong temperature gradients, re-circulation, and short-circuiting to name but a few.
- All free moisture and volatile matter entering the AAV takes part in the equilibrium calculation, though it could be expected that part of these would already be released in the freeboard.
- Only the C-fix content is varied, therefore the effects of volatile matter are ignored.
- Intense slag splashing is neglected, as are recirculating fumes and gases, and any solid feed affecting the arcing volume.
- No preheating or pre-reduction has taken place in the freeboard.

V. RESULTS AND DISCUSSION

A. *Scenario 1: Effect of Carbon and Temperature*

The results for calculated quantities when processing 26.2 tonne/h of feed mix are depicted in Figure 6. This graph shows the mass of all phases, and the compositions for slag, alloy, and process gas as a function of temperature and carbon additions to the feed mix.

Note in graph (a) in Figure 6 how first the smelting of solids leads to an increase in slag, and initially alloy disappears gradually then faster. The mass of gas increases about as much as the mass of alloy decreases, while the mass of slag only decreases slightly. Though the mass of slag remains fairly constant at a temperature over 1900 °C, the composition of slag changes significantly as shown in graph (b) in Figure 6: SiO_2 and MgO disappears mostly, while the mass of CrO increases strongly. Note for alloy in graph (c) how carbon decreases linearly with increasing temperature. The presence of chromium decreases once carbon has been reduced to a certain level, followed by iron once chromium has been reduced to less than half the original mass. Iron in alloy shows no noticeable variation for different RC values in graph (c), nor do H_2(g) and H(g) in graph (d). The formation of CO(g) and Mg(g) increases with both temperature and more carbon. Graphs (b), (c), and (d) show that once all carbon from an alloy is consumed, mainly the oxidation of chromium pushes the formation of Mg(g), Cr(g), and CrO(l).

Information on the composition of alloy in mass percent is given in Figure 7.

Note that in Figure 7 up to about 2100 °C the carbon content decreases while chromium and iron increase. Above 2100 °C the iron content increases as chromium from the alloy is used as a reductant and slagged. To get 8 pct or even 9 pct carbon in the alloy, temperature must be below 1800 °C and the RC above 2 pct. The plots are white above 2400 °C because this is where all alloy has been consumed as shown in graph(c) in Figure 6.

From the above various insights can be gained:

- From 1650 °C to 1750 °C and low-carbon additions the formation of gas, slag, alloy, monoxide and spinel remain fairly constant, but with high carbon additions alloy production slows down while the mass of gas and slag increases. MgO is already increasingly being reduced to Mg(g) below the slag tapping temperatures.
- From the slag composition in Figure 6 graph (b) in combination with Figure 6 graph(a) it can be deduced that from 1750 °C onward MgO and Al_2O_3 are released from the solid spinel and monoxide, while CrO in the slag starts to increase. Carbon additions affect the breakdown of the monoxide, but not significantly the breakdown of spinel.
- Slag continues to contain solids between about 1820 °C 1950 °C, depending on carbon additions.
- Between 1800 °C to 1950 °C mainly carbon from the alloy is consumed but, depending on carbon additions, also chromium, while the formation of slag and gas increases.

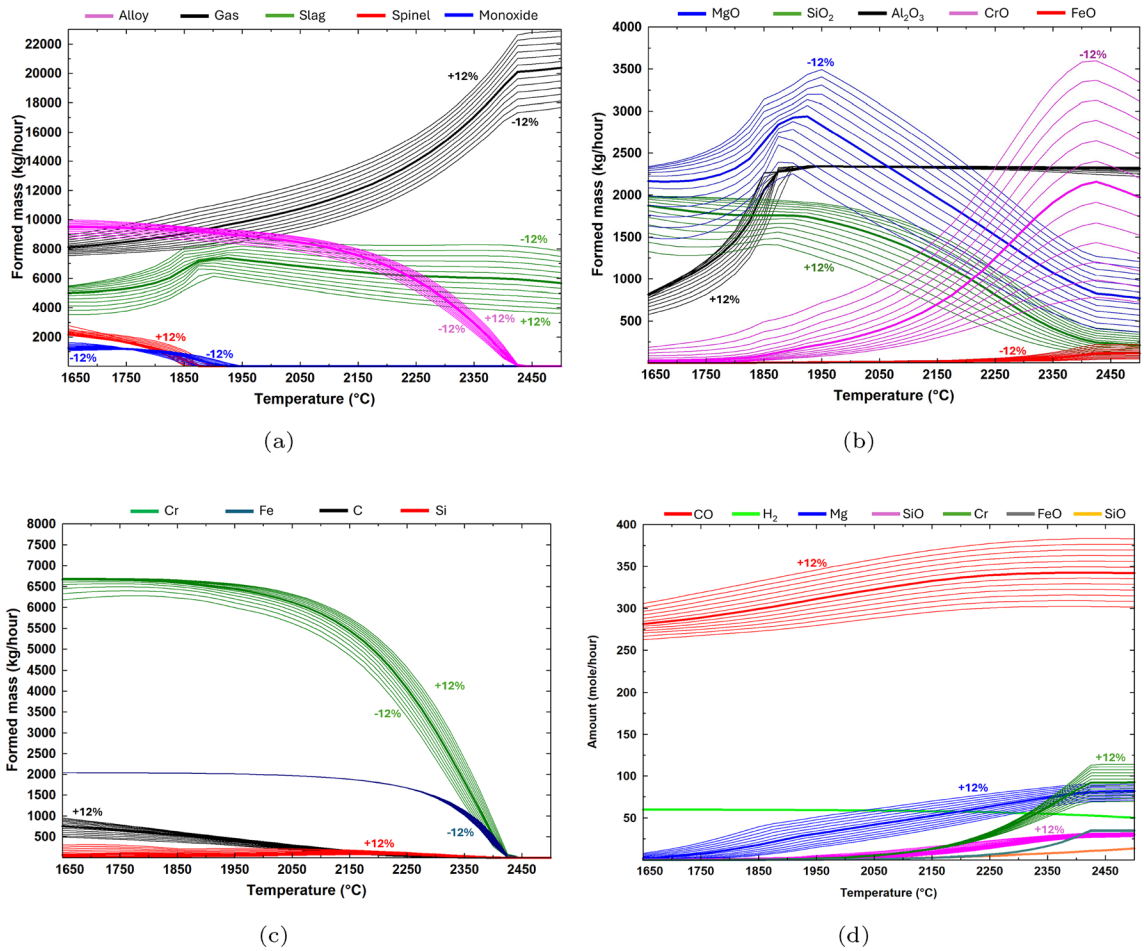

Fig. 6—Graphs showing the mass of all phases in (*a*), main slag components in (*b*), main elements in alloy in (*c*), and amount of main gas components in (*d*). The spread of the curves is a result of variation in RC in steps of 2 pct. For clarification, the curves for RC = 0 pct are made thicker, and to indicate the effect of RC on the equilibrium composition some values for RC are given in the graphs.

- The less carbon is present, the lower the temperature where chromium is slagged.
- The gas volume in Nm^3 nearly doubles from 1650 °C to 2500 °C , containing increasing masses of Mg(g), SiO(g), Cr(g), and mono-atomic H(g).

It appears that with an increase of temperature the alloy is used as a reductant for slag components, increasing the gas production, corroborating the observation of.[15] Additionally, it can be observed that the AAV of the FeCr DC furnace can operate like a carbothermic magnesium reduction reactor as described in.[38] The fact that no significant quantities Cr, Si, or Mg have been reported in actual furnace dust may be attributed to one or more of the following reasons:

- temperatures in the AAV are not as high as assumed in this analysis,
- feed material does not report to the AAV,
- Mg(g), Cr(g), and SiO(g) react in the freeboard with oxides, carbon, or water coming for example from feed materials or leaks from furnace cooling systems, or with water in gas cleaning,
- Mg(g), Cr(g), and SiO(g) condense and oxidize in the freeboard onto falling feed, on refractory,
- after the possible reactions mentioned, Mg(g), Cr(g), and SiO(g) flow as condensed or oxidized species back into the bath, or
- dust sampling and analyses are not done sufficiently to reveal where Mg(g), Cr(g), and SiO(g) go.

Doing more extensive dust analyses like particle sizing and mineralogical analyses (per size class) may reveal where Mg(g), Cr(g), and SiO(g) go.

1. *Furnace energy requirement*

This section looks deeper into the energy required for reaching the equilibria under different RC and temperature conditions in the AAV. An estimate for the industrial value for smelting the 26.2 tonne/h can be calculated using data given in Table III. With a feed rate of 26.2 tonne/h the charged mass of Cr_2O_3 is 9.8 tonne/h. Yessenzhulov[4] reported a recovery of 91.5 pct for chromium and an energy consumption of 4500 to 4700 kWh/t of FeCr. In calculating the energy consumption to process 26.2 $tonneh^{-1}$ based on the data above, following assumptions are made:

- the energy consumption is 4500 kWh/t of FeCr with a chrome content of 70 pct.

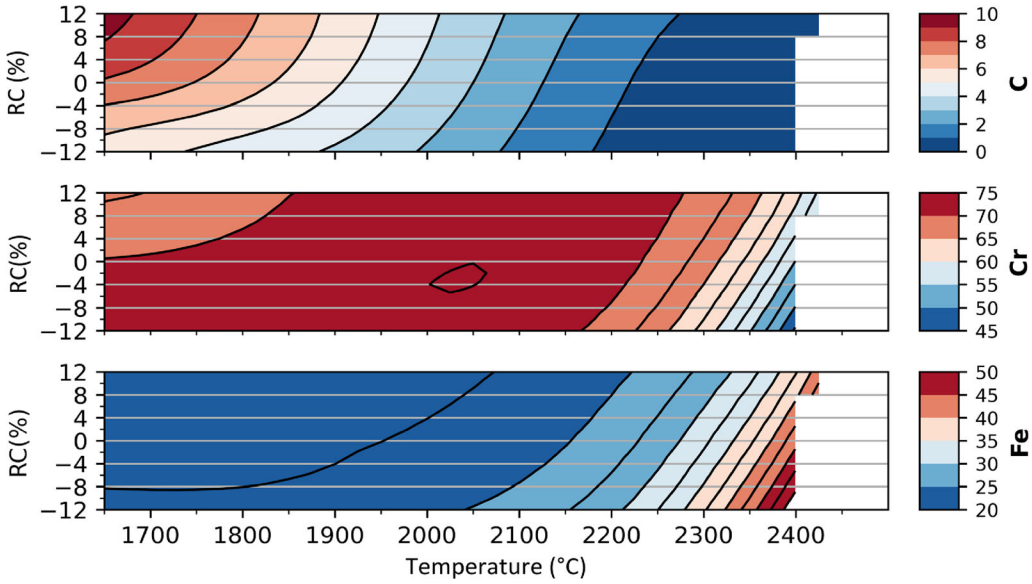

Fig. 7—Graphs showing the composition of the alloy in mass percent with C on top, Cr in the middle, and Fe on the bottom. The color bars give the mass percentage for each element. For Cr and Fe the thick lines in a color field represent half-way values (Color figure online).

- the 4500 kWh/t includes heat losses, and
- heat losses do not vary much depending on furnace load.

Combining these industrial data gives a required energy input of 39.6 $MWhh^{-1}$ to process the 26.2 t in 1.0 hour. Referring to Eq. [15] and with the energy consumption rounded up to 40.0 $MWhh^{-1}$ this gives an FTPR of 0.655 kg/kWh.

Results from FactSage for the energy requirement to smelt 26.2 t in 1.0 hour at different values for RC and at different temperatures is shown in Figure 8.

At an RC of 0 pct and a temperature of 1800 °C—the normal operation conditions shown by the black rectangle in Figure 8—the required energy is about 36 MWh. The dashed line represents a required energy input of 36 MWh to reach the calculated equilibria. This value does not include furnace heat losses. The calculated value for the required energy based on industrial data are 40.0 $MWhh^{-1}$ including heat losses, meaning that the 36 MWh from FactSage allow 4 MWh, or 10 pct, heat losses. The calculated value from FactSage therefore seems plausible. With 4 MWh of thermal losses, the entire area to the right of the dashed 36 MWh line is theoretically not possible with 40 MWh as furnace load, unless another source of energy is available. Possible mechanisms how more energy could be available in the AAV include:

- radiative and convective heat transfer from for example slag bath or freeboard into the AAV,
- gases, possibly formed in the AAV, preheat the falling feed in a counter-current heat exchange, or
- gases, possibly formed in the AAV, pre-reduce and preheat the falling feed in endothermic or even exothermic reactions.

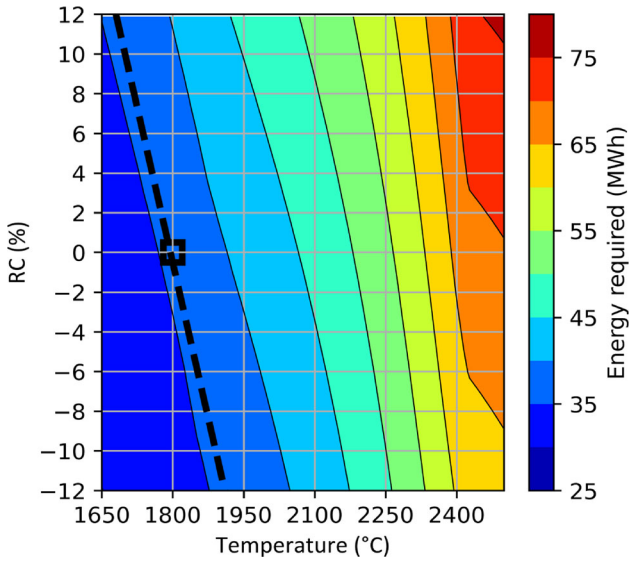

Fig. 8—Graph showing how RC and temperature affect the required energy to reach equilibrium. Note that increasing carbon in the feed mix increases energy consumption as endothermic reactions increase.

2. *Effect of carbon ratio, temperature, and partial oxygen pressure*

Figure 6 graph(d) shows that the main gases formed in addition to CO(g) are H_2(g), Mg(g), SiO(g), Cr(g), Fe(g) and H(g).

An important parameter is the partial oxygen pressure, given typically by Log(pO2). The dependency of $Log(pO_2)$ on temperature and carbon ratio is shown in Figure 9.

At the industrial slag tapping temperature of 1800 °C and RC = 0 pct the calculated $Log(pO_2)$ is −12.5. Every 150 °C increase raises the partial oxygen pressure by a factor of 10. A negative deviation of 10 pct in

carbon addition below about 1900 °C raises the partial oxygen pressure by a factor of 10. Negative deviations above 1900 °C and all positive deviations only raise the partial oxygen pressure by a factor of about 3, based on a change of around 0.5 on the logarithmic scale. The calculations show that in the AAV an increase in partial oxygen pressure can be expected, which can be explained by Le Chatelier's principle which tells us that increasing temperature will shift equilibrium for reactions like Eq. [13] to the left.

This effect of temperature on fuming can again be seen in Figure 10.

The calculations show that elevated temperatures, as can be expected near the electrode tip, strongly increase fuming of MgO and SiO_2 in spite of the higher partial oxygen pressure. The main reason is that the temperature drives the system towards reduction of MgO, SiO_2, and CrO using carbon and chromium as reductants. Figures 6 and 10 therefore indicate that above the slag tapping temperature of 1800 °C conditions are not favorable to formation of high carbon contents (>8 pct) in the alloy.

B. *Scenario 2: Effect of Slag and Temperature*

Slag can influence local equilibria in the slag bath where feed is introduced. This section investigates the effect of the slag mass that interacts with a fixed mass of feed material. 26.2 tonne of feed mix at ambient temperature is mixed with different masses of slag and the total is processed in 1.0 hour. The ratio $m_{slag} : m_{feed}$, called Alpha, is varied from 0 to 10 in equilibrium calculations. Quantity and composition for the feed are given in Table III and composition of the slag, at a fixed temperature of 1800 °C, is given in Table IV. Figure 11 shows the energy needed to reach equilibrium as a function of temperature and three different quantities of slag.

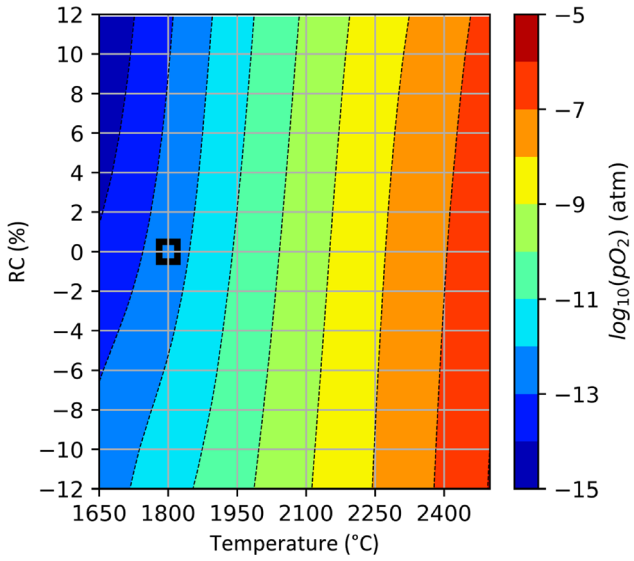

Fig. 9—Partial oxygen pressure in the AAV system as a function of temperature and carbon ratio. The point of industrial operation is given by the black square.

Note that the curve for Alpha = 0 is for a feed mix with a normal quantity of carbon (RC = 0 pct) being charged without any slag involved. The open circle on the curve for Alpha = 0 in Figure 11 shows that smelting feed at 1800 °C without slag requires about 36 MWh for the reactions. This value of 36 MWh is also given in Figure 8 by the black square at 1800 °C and RC = 0 pct.

Continuing with an available energy of 36 MWh for equilibrium reactions and Alpha = 4, then the open square shows that for Alpha = 4 and smelting at 1800 °C, only 24 MWh is required. This results in 36 MWh − 24 MWh = 12 MWh to be used elsewhere each hour, for example heating up of the bath, radiative heat transfer to the falling feed mix, or fume formation, to name a few. The filled square shows the point for Alpha = 4 and when all 36 MWh of energy is available for the equilibrium reactions. In that case, the temperature reaches approximately 1880 °C.

Similarly, but without symbol, if Alpha is 10, then 36 MWh allows equilibrium at 1900 °C.

Figure 11 also shows that:

- all scenarios with a different Alpha appear to intersect in a range of 39 to 40 MWh and 1925 °C to 1950 °C,
- below that area, more slag involved reduces the energy required to smelt the feed mix, and
- above that area, energy requirement increases faster the more slag is involved.

Summarizing, when slag is involved in the equilibrium calculations for feed mix at 36 MWh, then more slag allows a higher equilibrium temperature. However, there appears to be a limit, in the given case around 1925 °C, of the possible temperature increase that liquid slag can facilitate. The details of this mechanism may warrant further investigation but are beyond the scope of this paper.

Figure 12 shows the effect of increasing Alpha on the equilibrium masses of the main reaction products gas, slag, alloy, and solids.

Note that:

- as shown before, the thicker curves given by Alpha = 0 in Figure 12 are the same as the case for RC = 0 pct in Figure 6 graph(a),
- the quantity of added slag was so large, up to a ratio of 10 to 1, that only the curves for formed slag with Alpha = 0 and Alpha = 1 (upper-left corner) are visible in Figure 12 because of the maximum value chosen for the *Y*-axis,
- with an Alpha >1, alloy is fully consumed at lower temperatures as Alpha increases,
- with increasing Alpha, spinel continuous to be dissolved in slag around 1850 °C, but monoxide solids remain present at higher temperatures than with Alpha = 0, and
- as Alpha increases, formed gas and alloy both show non-linear behavior, where curves for different values

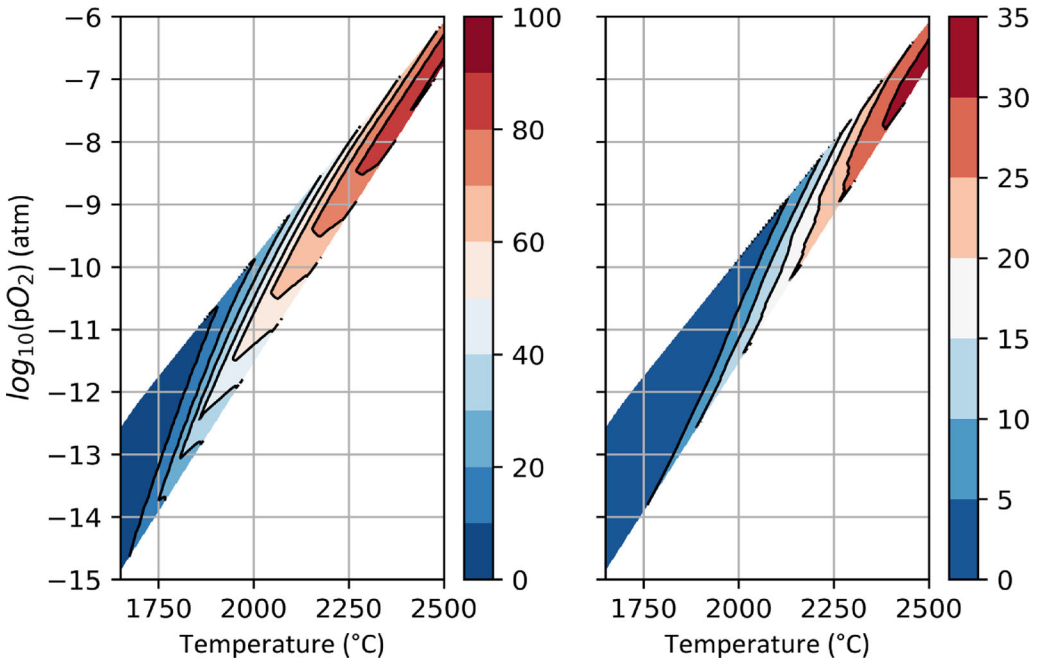

Fig. 10—Formation of Mg(g) (left) and SiO(g) (right) with the amount of formed gas in mole given by the color bar, where in both cases fuming increases with higher temperature and increased partial oxygen pressure. The boundaries of the region with data are determined by the used range of the carbon additions to the feed mix (Color figure online).

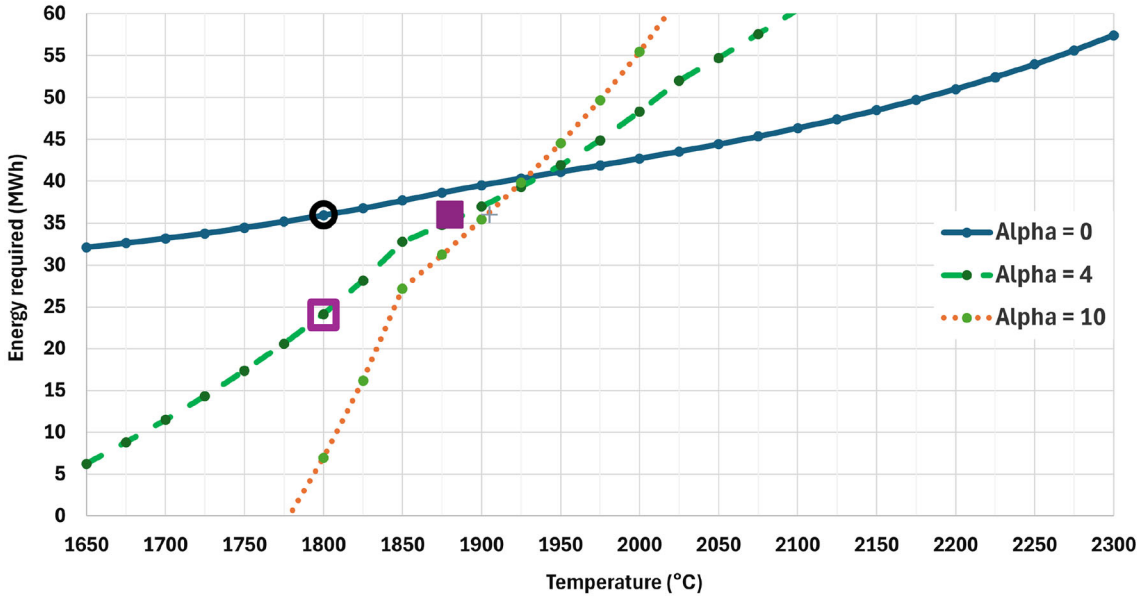

Fig. 11—Graph showing the effect of three different values of Alpha on the energy required to reach equilibrium. The meaning of the squares and circle is explained in the text below this graph.

of Alpha cross each other, unlike for example monoxide.

What can be seen is that the quantity of formed alloy becomes less as more slag is interacting with the feed mix. Assuming there is a constant mass of slag involved in the equilibrium reactions in the AAV at a certain furnace load set point, then the feed mix charged as given by the FTPR would affect alloy formation, because Alpha is changed. Such a detail may not be noticed if a more black-box approach is followed, which obfuscates the hidden mechanisms inside the furnace. How much slag is actually involved in the AAV equilibrium reactions may depend on slag viscosity, slag bath depth, furnace load, and electrical setpoints like current or resistance.

The development of the masses of the main alloy forming elements Cr, Fe, and C depending on temperature and Alpha is shown in Figure 13.

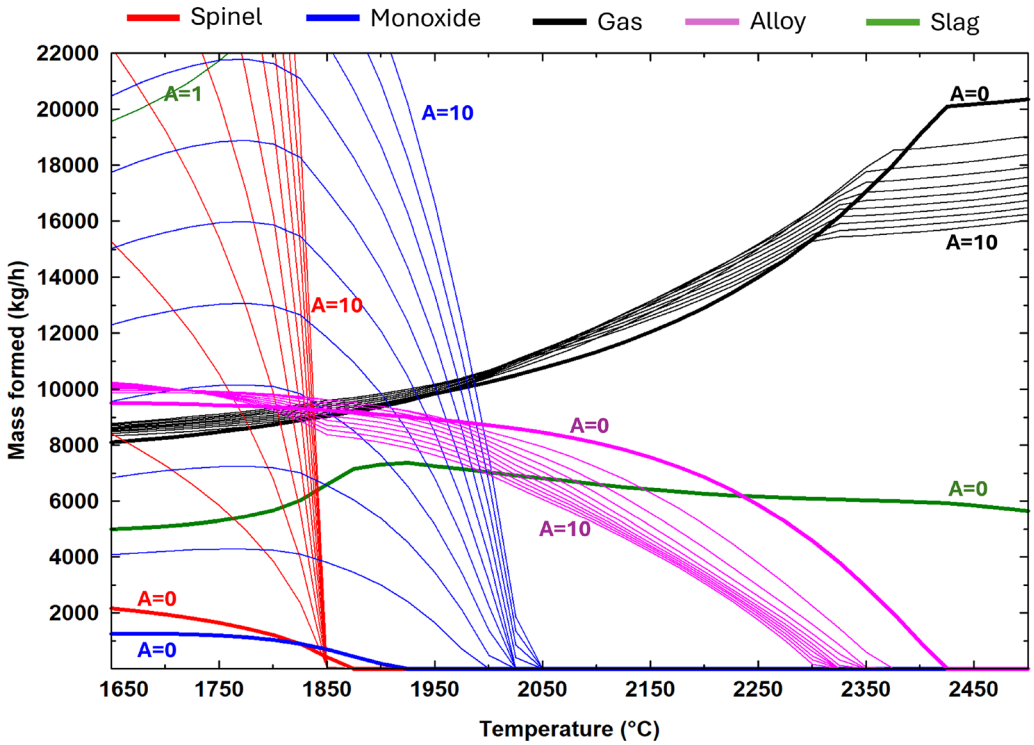

Fig. 12—Thick lines represent Alpha = 0 and Alpha increases in steps of 1. For all phases two values for Alpha are given to identify how the formation of masses is affected by changing Alpha.

The carbon content of alloy decreases with increasing temperature because the carbon is used to reduce oxides from slag. This is accelerated when Alpha increases as more slag is available for reduction. Increasing Alpha means that more Fe- and Cr-oxides are available in liquid slag for reduction by the formed alloy. At ratios for Alpha <2, carbon is used to reduce both Cr- and Fe-oxides from the slag, as can be seen by the increase in mass of chromium and iron. When Alpha reaches a value of 3, the mass of Fe-oxide in the liquid slag is so much that the carbon is insufficient to reduce both Cr- and Fe-oxides, and chromium is also used as a reductant for the Fe-oxide. As a result, the alloy is depleted from chromium and enriched in iron. Once the carbon has neared depletion, then iron in the alloy becomes a reductant for MgO in the slag as well and is consumed until no more alloy is left.

Figure 14 shows in a different way how temperature and Alpha over the selected range change the alloy composition, given in mass percent for different elements.

With increasing temperature and Alpha = 0, carbon is removed by slag components and an alloy with a significant percentage of chromium remains until all the alloy is gone. The more slag is added to the system, the more chromium from the alloy is used to reduce Fe-oxides from the feed and especially liquid slag. This mechanism leads to an alloy increasingly rich in iron and poorer in chromium, until at some point all alloy is used. Take special note that even with Alpha = 0 and at 1650 °C the carbon content is below 8 pct. How the alloy is consumed can be deducted by looking at Figure 14 in combination with Figure 15.

Based on the information from Figure 15 and in combination with Figures 12, 13, and 14 following observations can be noted:

- With slag participating in the equilibrium calculations, the formation of Mg(g) is suppressed up to about 2000 °C due to the available Fe- and Cr-oxides in the added slag at sufficient high activity.
- Carbon from alloy is used to reduce Fe- and Cr-oxides as can be seen by the increased amount of formed CO(g).
- Above 2000 °C the formation of Mg(g) is increased strongly as the increased mass of MgO(l) in slag is reduced by chromium and later iron.
- Notably, a maximum of Mg(g) formation takes place at Alpha = 4 and a further increase of Alpha leads to a reduction in Mg(g) formation.
- A similar trend can be seen for SiO(g) where Alpha = 1 increases SiO(g) formation, but higher values for Alpha reduce SiO(g) formation.
- Formation of Cr(g), SiO(g), and Fe(g) is generally suppressed by the presence of more slag.

A thermochemical equilibrium analysis was done with a fixed charging rate of feed mix, while increasing the mass of liquid slag involved and varying temperature. Slag has a significant impact on the final equilibrium:

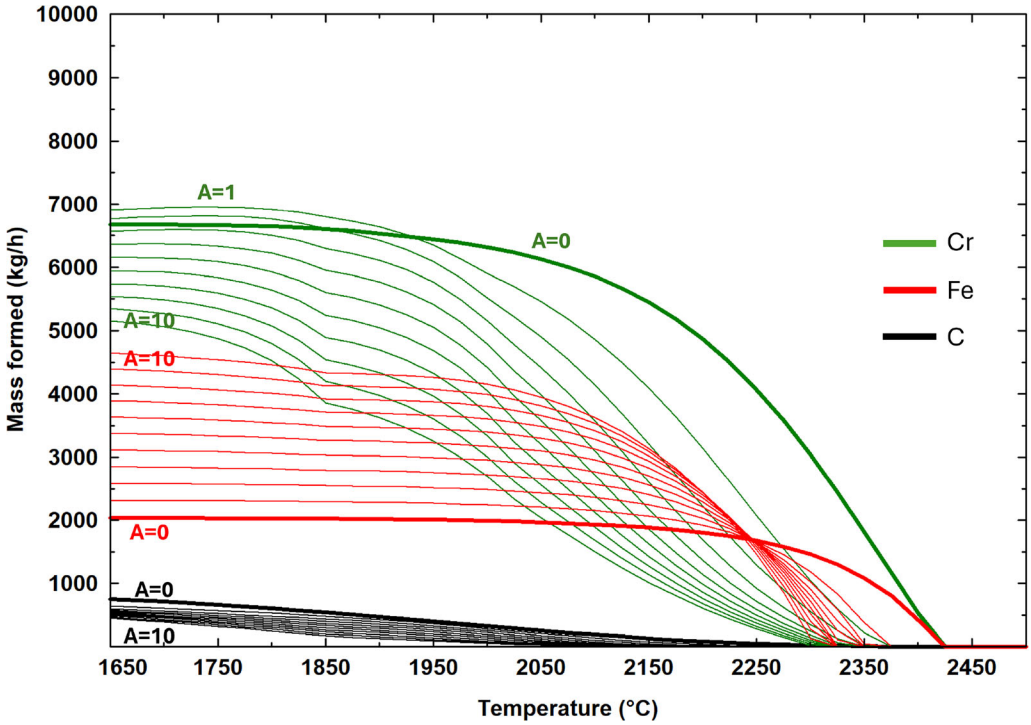

Fig. 13—Lines with the same color represent the equilibrium masses at different values for Alpha. Alpha changes in steps of 1 and at least two values for Alpha are shown in the graph to identify how Alpha affects the alloy composition.

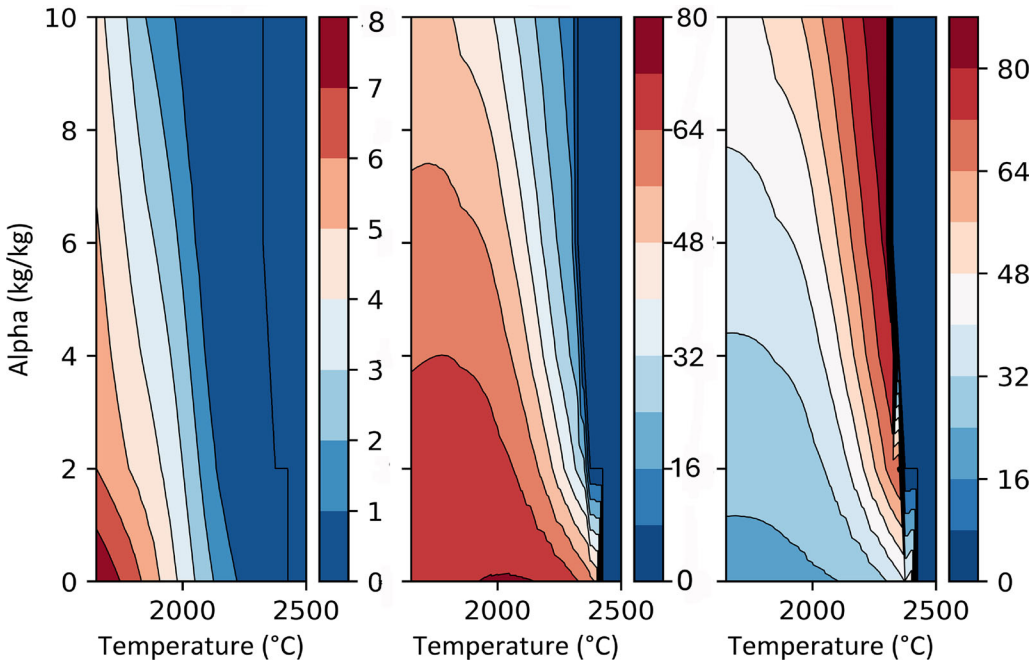

Fig. 14—Graphs showing the composition of formed alloy with C (left), Cr (center), and Fe (right). Each graph has a color bar showing the mass percentage of the respective element. Alpha on the *y*-axis is valid for all three graphs (Color figure online).

- A higher value for Alpha leads to a reduction in alloy production, as alloy is used in reduction of mainly MgO(l) from the additional slag.
- A higher value for Alpha allows higher equilibrium temperatures when the energy input is fixed, but there appears to be a limit around 1950 °C.
- Around 1950 °C the formation of Mg(g) increases notably, as well as the energy required to reach the equilibrium composition as shown in Figure 11.
- Though higher equilibrium temperatures allow dissolution of spinels, which means less suspended solids

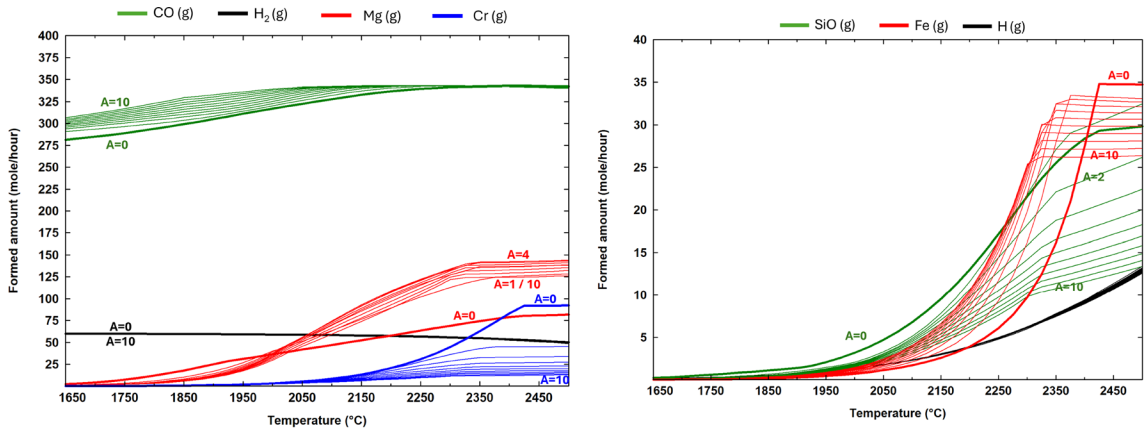

(a) (b)

Fig. 15—Graph (*a*) and (*b*) show the amount of moles for the main components of formed gas. For clarity, graph (b) shows the smaller components SiO(g),Fe(g), and H(g) that can not be seen properly in graph (a). Different lines with the same color represent the equilibrium amount at different values for Alpha. Alpha changes in steps of 1 and at least two values for Alpha are shown in the graph to identify how Alpha affects the gas composition. For Mg(g), Alpha values from 1 to 4 increase but with higher values decrease the formation of Mg(g) (Color figure online).

in slag, this effect is countered by an increased presence of monoxide solids in suspension.

This leads to the possible postulation that the formation of Mg(g) acts as a damper on the system. If not enough feed mix is charged, then the ratio slag-to-feed increases, meaning more energy and MgO is available for reactions between slag and alloy to occur. This leads to an increased formation of Mg(g), dissipating the surplus of energy and keeping the temperature rise of the reaction zone limited.

C. *Exergy Evaluation of the AAV*

As shown in the fundamental thermodynamic analysis in the previous sections, it is clear that a large amount of process gas is formed, containing species like CO(g), H2(g), Mg(g), SiO(g), Cr(g), Fe(g), and H(g). It has also been shown in Figures 8 and 11 that in the selected ranges for RC, Alpha, and temperature many equilibria are not possible when there is a limit on the available energy.

The mentioned gaseous species formed in the AAV could provide that energy.

To evaluate the chemical potential energy of these gaseous species an exergy evaluation is done. ''Exergy gives an idea of the quality of resources such as energy, water, or raw materials'', Handbook of Recycling.[51] It more importantly provides insight into the losses due to irreversibilities in the reactor, based on the standard state derived from species in the earth crust, sea water, and atmosphere. Therefore, in this analysis, the exergy distribution over alloy, slag, and gas is calculated to understand how its magnitude and distribution change under different conditions relative to these standard states of the elements. This provides and guides thoughts, where the process can be optimized. Exergy data are calculated using HSC,[52] which has incorporated the standard state data as derived by Szargut[53] as described in the cited chapter 11 of the 2nd edition of the Handbook of Recycling. Results from HSC and FactSage can be slightly different because HSC does not fully embrace solution chemistry. However, by applying the calculated output streams from FactSage in HSC, similar results can be obtained for the energy requirement to reach equilibrium.

Nine different scenarios are chosen to do equilibrium calculations in both FactSage and HSC on a feed mix as given in Table III with a feed rate of 26 tonneh^{-1} as based on a power input of 40 MWh. The variables are:

- RC values of −12, 0, and 12 pct, and
- temperatures of 1800 °C, 2150 °C, and 2350 °C

The energy requirement to reach equilibrium with both HSC and FactSage is shown in Figure 16, revealing if HSC is used well, there is good reproducibility of data obtained using FactSage.

A difference can be seen, but the effect of solution chemistry seems to be small and does not prevent the use of HSC for exergy calculations to derive useful insights.

Nine cases are shown in Figure 17, where the rounded exergy values are shown for:

- feed materials,
- electrical energy needed to reach equilibrium,
- process gas,
- slag, and
- alloy.

The required energy to reach equilibrium is calculated with FactSage, while the exergy content of all material streams is calculated with HSC.

The exergy calculated for feed materials changes depending on the quantity of carbon in the mix:

- 41 MWh when the RC is 12 pct below the normal recipe,
- 46 MWh when the RC is as in the normal recipe, and

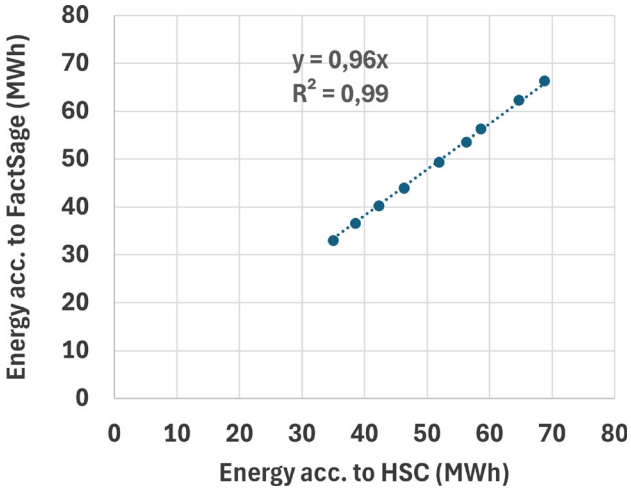

Fig. 16—Comparison of the energy requirement calculated by HSC and FactSage, respectively, to reach equilibrium for nine selected variations on temperature and RC.

- 50 MWh when the RC is 12 pct above the normal recipe.

The required electrical power input to reach equilibrium is different for each scenario and given underlined in the boxes under the electrodes, for example 33 MWh in the top left image. By definition, electrical energy is equal to exergy input. Note the increasing difference between actual energy input of 40 MWh for a feed rate of 26 tonneh^{-1} and the required energy input to reach equilibrium under the given temperature and RC conditions.

In the top left image, exergy values for process gas are given in the freeboard (29 MWh), and the values for slag (7 MWh) and alloy (30 MWh) are depicted in the slag and alloy baths, respectively. The exergy content for process gas includes only Mg(g), SiO(g), Cr(g), Fe(g), H(g), CO(g), and H2(g). For the top left image this results in an exergy efficiency of 90 pct, as shown in Figure 17.

$$\text{Exergy efficiency } \eta(\text{pct}) = 100 * \frac{29+7+30}{41+33}\left(\frac{\text{MWh}}{\text{MWh}}\right) = 90\,\text{pct} \quad [17]$$

Figure 17 for this novel analysis of the AAC uniquely shows that:

- in all but two cases the equilibrium can be met only if additional energy is available in the AAV, coming for example from energy contained in process gas,
- the exergy content of process gas increases strongly with increasing temperature and carbon ratio,
- a large part of the exergy is contained in CO(g) and H2(g), and leaves the AAV and the furnace for potential use elsewhere,
- though the exergy content of CO(g) increases with temperature and carbon additions, its relative contribution to the total exergy decreases, and
- the increase in exergy originates mainly from Mg(g), SiO(g), Cr(g), and Fe(g), which can react inside the furnace to fully utilize the irreversibility of these reactions to reach a more stable state.

The changes of exergy content in slag, alloy, and process gas for RC = 0 pct. and at three selected temperatures are shown in Figure 18 to visualize the change of exergy over alloy, gas, and slag at different temperatures.

With a focus on irreversibility the exergy analysis shows that:

- the process gas has a very high exergy value, therefore a very high chemical potential energy content,
- the contained exergy can be used within the furnace, and
- the exergy value for process gas increases dramatically when temperatures in the AAV increase, alluding to the significant irreversible losses in the furnace that will affect productivity and economic viability for such a scenario.

This strengthens the conclusion of the exergy evaluation that a substantial quantity of energy is available in process gas, and that this increases significantly with increasing temperature in the AAV.

An important conclusion therefore is that the quantity of carbon in the feed mix has less of an impact than an increase in temperature, as can be seen in Figure 19. The temperature drives significant irreversible reactions, which are not beneficial for optimal furnace operation.

Figure 19 uniquely shows that:

- more carbon charged with the feed increases the exergy content of the gas, but
- an increase in temperature has a far bigger effect due to its effect on the additional formation of Mg(g), SiO(g), Cr(g), Fe(g) and H(g) caused by consumption of alloy as a reductant.

For scenario 2, no exergy analysis is included for brevity and results may be different due to the involvement of increasing quantities of slag. Thermochemical calculations already showed that the formation of Cr(g) and SiO(g) is suppressed but the more Mg(g) is formed the more slag takes part in the equilibrium reactions.

Concluding, similar to energy is that with increasing temperature exergy is increasingly dominant in the gas phase, which by design is destined to leave the furnace. To minimize exergy losses and energy consumption, all should be done to use as much of the MWh contained in the formed process gas as possible, and especially manage the temperature in the AAV by flow of materials into the zone. How, where, and how much of what material is charged is highly important in control and optimization of a DC furnace.

VI. DISCUSSION AND CONCLUSION

This investigation clearly shows that the AAV is a significant zone in a DC arc FeCr furnace.

Some specific observations focusing on the AAV:

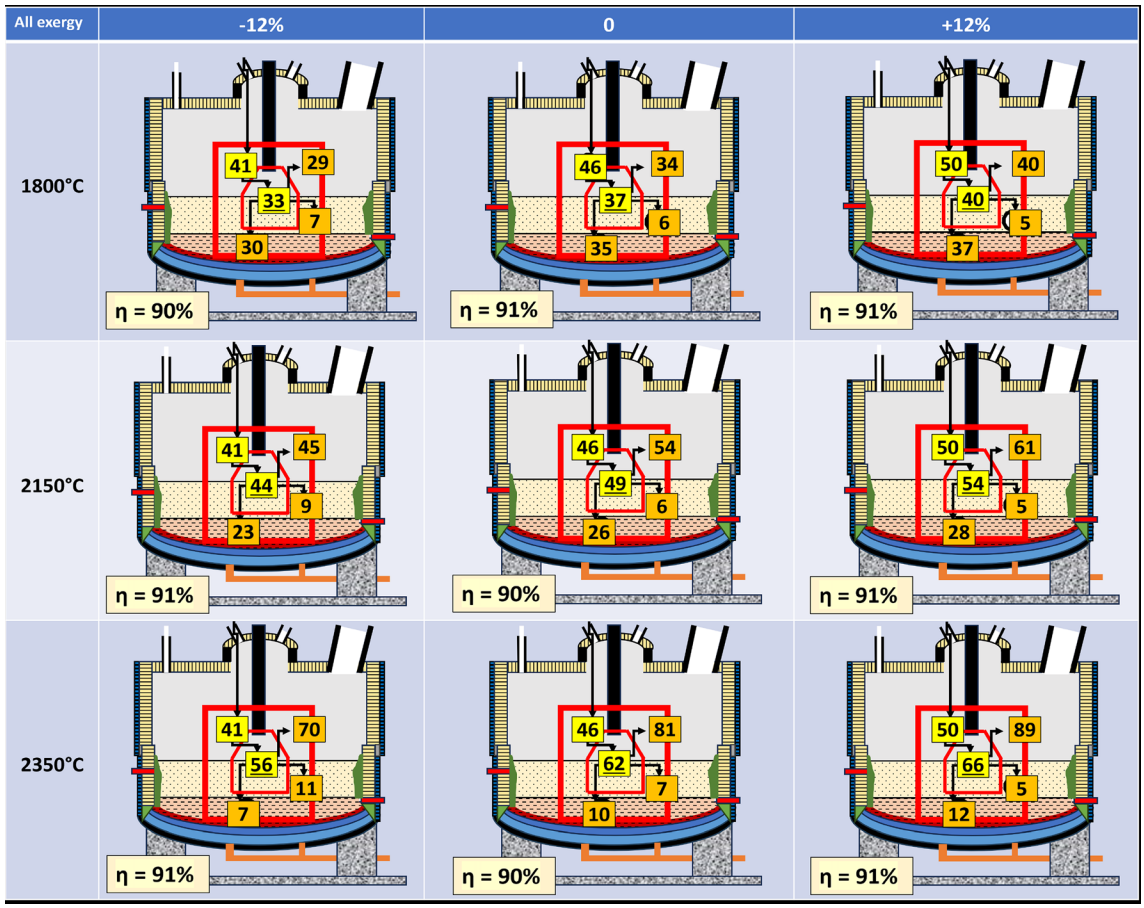

Fig. 17—Absolute exergy distribution from the AAV for the nine selected variations on temperature (1800 °C, 2150 °C, 2350 °C) and carbon ratio (−12 pct, 0 pct, +12 pct). Note especially how the exergy for evolved gas increases significantly. The exergy efficiency for each scenario is given by η.

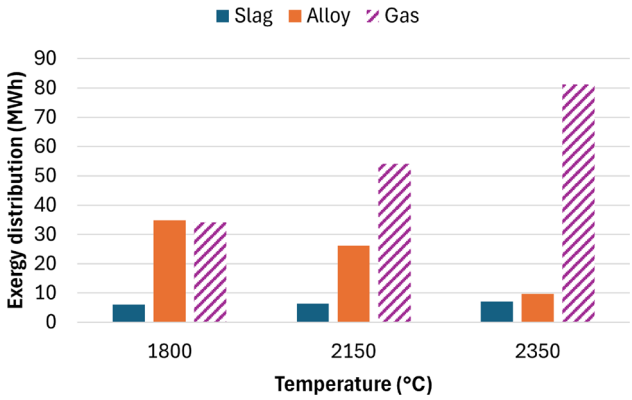

Fig. 18—Absolute exergy distribution over slag, alloy, and gas phase for RC = 0 pct and at different temperatures.

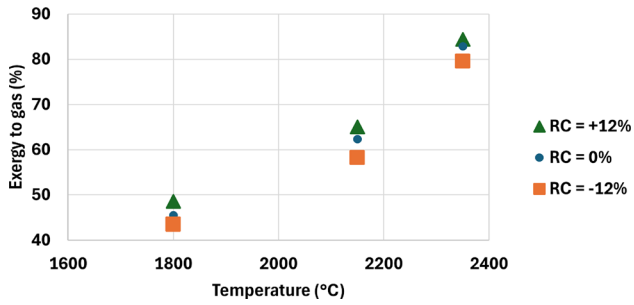

Fig. 19—Percentage of exergy going to the gas phase as a function of carbon ratio and temperature. Note that the effect of temperature is more important than the effect of carbon.

- **Alloy composition** The investigated carbon ratios, slag ratios, and temperatures cannot explain the high carbon contents in the alloy as encountered industrially. The formation of FeCr with carbon contents of above 8 pct or even 9 pct seems difficult unless carbides are formed below the slag tapping temperature of 1800 °C while RC values are above the normal value of RC = 0 pct. The carbides then still need to pass through the slag without reacting with it. However, it is shown that the more slag is available, the faster carbon is refined from formed alloy, which argues against large volumes of slag being involved in the equilibrium reactions.
- **High AAV temperatures** Even if the bulk slag temperature interacting with the AAV zone is as low as the tapping temperature of 1800 °C, then mixing of slag and feed allows for a higher temperature in the AAV, which affects composition and viscosity of the slag. If all feed is smelted above 1950 °C in the case of

Alpha = 0, or above 2050 °C when Alpha ≥ 1, it is shown that there are no suspended solids present anymore. This implies that viscosity related tapping problems due to slurry formation can depend on formation of the first solid compounds in slag and not melting of the last feed solids that have yet to melt. With increasing AAV temperatures, more gases form, and more MWh can be transferred by fumed slag components to the falling feed. If this energy transfer takes place, thermochemical equilibria in the AAV can be reached well above the theoretical limit given by the electrical power input into the AAV. A deeper consideration of freeboard reactions is required to verify if the concept of freeboard preheating and pre-reduction is valid.

- **High exergy of gas from the AAV** It is important to know the energy content of material streams in a process (thermal and chemical). However, if this energy cannot be used due to its low quality, this is a true operational issue. This paper shows the importance of understanding gas formed in the AAV in reducing exergy dissipation. Higher values for RC increase gas formation, initially only CO(g) and Mg(g), but from 2150 °C upward Cr(g), SiO(g) and even Fe(g) are formed. Increased presence of slag on the other hand suppresses formation of especially Cr(g) and SiO(g) though more Mg(g) is formed. The exergy analysis confirms that to ensure minimal waste of both thermal and chemical energy, a deeper understanding and improved furnace operation should be implemented to help recover energy from fumes such as Mg(g), SiO(g), Cr(g), and Fe(g) before process gas leaves the furnace. This would also include volatile species Cl and S containing species that are not considered in this analysis. Understanding how to harness both chemical and thermal energy flows in terms of exergy in the furnace is of critical importance. The interaction between gases and feed mix falling through the freeboard is of significance in this regard. The possible energy transfer by fumes to falling feed may play a similar mechanistic role in other DC smelting processes with very different outcomes due to the presence of different components, such as CaO, Ni, or Fe, that are present in different quantities.
- **Volatile gas species from the AAV in steel production** This paper provides some significant insights into the phenomena that can assist in understanding how to reduce energy consumption in DC FeCr production. The importance of fuming of volatile compounds and elements and their consequences may be of particular interest for both AC and DC open-bath smelting processes under investigation for the decarbonization of steel. Note that steel slags typically contain some MgO and are high in SiO_2, which both can be fumed.

It is also clear from the analysis in this paper, that the AAV interacts with the other zones in the furnace. Work has already been published, how the AAV interacts with other zones by the application of a dynamic model to better understand the effect of the interactions. To explore the implications of the results of the paper and to develop further insights, the following is being evolved:

- Further refining a multi-zone dynamic process model to fully understand the interactions between the zones postulated in this paper.
- With the aid of the multi-zone simulation model significant insight and understanding (pre-reduction) reactions in the freeboard can be obtained. This specifically focuses on the interaction of process gas emitted from the AAV with solids in the freeboard zone, and the consequences on the smelting process.
- The interactions between the zones and the subsequent effect of spinel and other created solids in slag formation on gas evolution needs to be understood. This may lead to foaming of slag and affect tapping as well as the general movement of slag in the furnace.
- It is clear that the gas phase evolving from the AAV has a significant effect on the transport of energy as chemical potential and thermal energy. This is a significant neglected aspect overlooked in computational fluid dynamic studies that focus more on the energy balance of the arc with a focus on radiation, convection, and conduction, neglecting the significant flow of energy in the material flows.

In summary, to better understand how the phenomena that occur in the AAV affect furnace operations, a dynamic model will be further evolved that connects the nine zones. Calibration will occur by also considering specifically the particle size distribution of the furnace dust and chemically analyze the different fractions to link these back to the AAV. Additionally, analyses of rapidly quenched slag samples will provide information on the presence of viscosity increasing solid particles, be it partially altered chromite or precipitates. This will discern between normal carry over and chemically formed compounds after volatilization and subsequent oxidation and therefore be a significant marker for furnace efficiency and hence losses due to numerous hidden irreversibilities in the zones.

CONFLICT OF INTEREST

On behalf of all authors, the corresponding author states that there is no conflict of interest.

OPEN ACCESS

REFERENCES

1. H. Fuchs: Untersuchung des petrographischen und mineralogischen Aufbaues von Chromerzen fur die metallurgische Verwertung und ihrer Reduzierbarkeit mit dem Ziel der Aufstellung von Bewertungsrichtlinien. Ph.D. Thesis, RWTH Aachen, Germany, 1962.
2. A. Pershukov, N. Tagirov, and G. Ekhlakova: *Gorni Zhurnal*, 1991, vol. 11, pp. 7–10.
3. M. Ford and J. Oosthuizen: The production of ferrochromium in a 40 MVA DC plasma furnace. Paper presented at the 7th Infacon, Trondheim, Norway, 11–14 June 1995.
4. A. Yessenzhulov and E. Abdulabekov: The new and reconstructed facilities at the enterprise TNK Kazchrome JSC. Paper presented at the conference The best available technologies for steel and ferroalloys production, 14 October 2020.
5. GTT. https://gtt-technologies.de/software/factsage/. Accessed 28 Aug 2024.
6. I. Geldenhuys: Aspects of DC chromite smelting at Mintek: an overview. Paper presented at the 13th Infacon, Almaty, Kazakhstan, 9–13 June 2013.
7. E. Shotanov, A. Roshchin, V. Panfilov, N. Nurgali, and M. Dossekenov: *Metallurgist*, 2022, vol. 66, pp. 871–80.
8. H. Kammeyer, K. Maske, and G. Pugh: Open bath production of ferrochromium in a DC plasma furnace. Paper presented at the 5th Infacon, New Orleans, USA, 23–26 March 1989.
9. O. Sariev, B. Kelamanov, Y. Zhumagaliyev, S. Kim, A. Abdirashit, and M. Almagambetov: *Metalurgiya*, 2020, vol. 59, pp. 533–36.
10. D. Sager, D. Grant, R. Stadler, and T. Schreiter: Low cost ferroalloy extraction in DC-arc furnace at Middleburg Ferrochrome. Paper presented at the 12th Infacon, Helsinki, Finland, 6–9 June 2010.
11. R. Jones and M. Erwee: *CALPHAD: Comput. Coupling Phase Diagr. Thermochem.*, 2016, vol. 55, pp. 20–25.
12. C. Kempe, A. Haaks, A. Scheltema Beduin, A. Liedtke, and H. Oterdoom: Bath level measurement for a closed DC furnace. Paper presented at the Conference of Metallurgists, Toronto, Canada, 23–26 August 2015.
13. R. Degel, C. Froehling, M. Koeneke, E. Hecker, H. Oterdoom, and A. Van Niekerk: History and new milestones in submerged arc furnace technology for ferro alloy and silicon production. Paper presented at the 14th Infacon, Kiev, Ukraine, 31 May–4 June 2015.
14. C. Kempe, A. Liedtke, A. Haaks, H. Oterdoom, and A. Scheltema Beduin: The SMS-group DC electrode column (cathode), design, and operation. Paper presented at the Conference of Metallurgists, Vancouver, Canada, 27–30 August 2017.
15. N. Barcza, T. Curr, and R. Jones: *Pure Appl. Chem.*, 1990, vol. 62, pp. 1761–72.
16. Z. Yan, T. Htet, J. Hag, K. Meijer, and Z. Li: *Metall. Mater. Trans. B*, 2021, vol. 54B, pp. 868–79.
17. A. Schei, J. Tuset, and H. Tveit: *Production of High Silicon Alloys*, Tapir, Trondheim, 1998.
18. D. Swamy and D. Roberston: Factors affecting carbon consumption in the production of high carbon ferro manganese. Paper presented at the 9th Infacon, Quebec City, Canada, 3–6 June 2001.
19. S. Olsen, M. Tangstad, and T. Lindstad: *Production of Manganese Ferroalloys*, Tapir, Trondheim, 2007.
20. D. Robertson. The computation of the kinetics of reactions between multiple phases. Paper presented at the EPD congress, Point Clear, California, 12–15 November 1995.
21. S. Ohguchi, D. Robertson, B. Deo, P. Grieveson, and J. Jeffes: *Ironmak. Steelmak.*, 1984, vol. 11, pp. 202–357.
22. M. Van Ende: *JOM*, 2022, vol. 74, pp. 1610–23.
23. J. Rezende, R. Van Schalkwyk, M. Reuter, and M. To Baben: *J. Sustain. Metall.*, 2021, pp. 964–77. https://doi.org/10.1007/s40831-021-00387-7.
24. H. Oterdoom, M. Reuter, and J. Zietsman: The importance of understanding mechanisms in open-bath (DC) processes related to furnace containment. Paper presented at the 2024 TMS Conference, Orlando, 4–7 March 2024.
25. J. Koster: in *Studies on the Treatment of Domestic Chrome Ores. Progress Reports—Metallurgical Investigations*, J. Koster, S. Shelton, and R. Knickerbocker, eds., United States Bureau of Mines, 1936, pp. 3–27.
26. F. Wessel and R. Rasmussen: *JOM*, 1950, pp. 984–88. https://doi.org/10.1007/BF03399093.
27. S. Taneka and D. Robertson: Carbothermal reduction of friable chromite in a small-scale transferred-arc furnace. Paper presented at Pyrometallurgy '87, London, England, 21–23 September 1987.
28. Mintek. https://www.pyro.co.za/Mintek/Pyrosim/Pyrosim.htm. Accessed 28 Aug 2024.
29. J. Eksteen, S. Frank, and M. Reuter: *Miner. Eng.*, 2002, vol. 15, pp. 931–43.
30. E. Berryman and D. Paktunc: *J. Hazard. Mater.*, 2022, vol. 422, pp. 1097–1104.
31. E. Berryman, D. Paktunc, D. Kingston, and J. Beukes: *Clean. Eng. Technol.*, 2022, vol. 6. https://doi.org/10.1016/j.clet.2021.100386.
32. B. Bowman: Properties of arcs in DC furnaces. Paper presented at the 1994 Electric Furnace Conference, Nashville, 13–16 November 1994.
33. W. Hunter and L. Banning: Electric smelting of Montana chromite concentrates. Report of investigations 5775.
34. K. Suzuki and K. Mori: *Trans. Natl. Res. Inst. Met.*, 1980, vol. 20, pp. 607–13.
35. O. Demir and R. Eric: The reduction of chromite in Fe-Cr-C-Si alloys. Paper presented at the 6th Infacon, Cape Town, South Africa, 8–11 March 1992.
36. B. Tsomondo, D. Simbi, and L. A: Kinetic investigation of chromite reduction in a high-carbon ferrochromium alloy bath. Paper presented at the 7th Infacon, Trondheim, Norway, 11–14 June 1995.
37. G. Volkert and K.-D. Frank: *Metallurgie der Ferrolegierungen*, 2nd ed., Springer Verlag, Heidelberg, 1972.
38. A. Cameron, J. Lotens, C. Ouwehand, and V. Aurich: Carbothermic production of magnesium. Paper presented at Pyrometallurgy '87, London, England, 21–23 September 1987.
39. M. Abdellatif: Pilot plant demonstration of the Mintek thermal magnesium process. Paper presented at the international symposium on magnesium technology, Conference of Metallurgists, Montreal, Canada, 1–4 October 2006.
40. M. Cyr, A. Carles-Gibergues, and A. Tagnit-Hamou: *Cem. Concr. Res.*, 2000, vol. 30, pp. 1097–104.
41. N. Rughubir and D. Bessinger: Furnace dust from Exxaro Sands KZN. Paper presented at the 6th international symposium Heavy Minerals Conference, South Africa, 1–4 October 2007.
42. M. Khesa: The characterization and carbothermic reduction of furnace dust from the TKZN heavy mineral sands operation. Master's Thesis, University of Pretoria, South Africa, 2016.
43. Helios. Adoption of hydrogen metallurgy in the climate-neutral production of steel. https://helios-dn.eu/. Accessed 7 Jan 2024.
44. D. Ernst, M. Zarl, M. Farkas, and J. Schenk: *Steel Res. Int.*, 2023, vol. 62, pp. 43–49.
45. P. Behera, B. Bhoi, R. Paramguru, P. Mukherjee, and B. Mishra: *Metall. Mater. Trans. B*, 2019, vol. 50B, pp. 262–70.
46. Helios. DC5 hydrogen plasma-based reduction of chromite/chromium oxide for stainless steel production. https://helios-dn.eu/dc5/. Accessed 7 Jan 2024.
47. J. Moore, K. Reid, and J. Tylko: *JOM*, 1981, vol 62, pp. 43–49.
48. D. MacRae: in *Application of Plasma Technology to Ferroalloy Processing. Plasma Technology in Metallurgical Processing*, J. Feinman, ed., Iron and steel society, Warrendale, 1987, pp. 149–161.
49. I. Sommerville, A. McLean, and C. Alcock: in *Materials Processing in Plasma Furnaces Equipped with Graphite Electrodes. Plasma Technology in Metallurgical Processing*, J. Feinman, ed., Iron and steel society, Warrendale, 1987, pp. 89–101.
50. O. Privalov, Y. Abdulabekov, Z. Nurmukhanbetov, M. Kospanov, and Z. Mussabekov: Adjustment of high carbon ferrochrome

composition in DC furnaces. Paper presented at the 13th Infacon, Almaty, Kazakhstan, 9–13 June 2013.
51. A. Llamas Abadia, N. Bartie, C. Meskers, and M. Reuter: *Handbook of Recycling*, 2nd ed., Elsevier, Amsterdam, 2024.
52. METSO. https://www.metso.com/portfolio/hsc-chemistry/. Accessed 28 Aug 2024.
53. J. Szargut: *Appl. Energy*, 1989, vol. 32, pp. 269–86.